arXiv:astro-ph/9912310v2 16 May 2000

Age–luminosity relations for low-mass metal-poor stars

A. Weiss and H. Schlattl

Max-Planck-Institut für Astrophysik, Karl-Schwarzschild-Str. 1, 85748 Garching, Federal Republic of Germany

Abstract. We present a grid of evolutionary calculations for metal-poor low-mass stars for a variety of initial helium and metal abundances. The intention is mainly to provide a database for deriving directly stellar ages of halo and globular cluster stars for which basic stellar parameters are known, but the tracks can also be used for isochrone or luminosity function construction, since they extend to the tip of the red giant branch. Fitting formulae for age-luminosity relations are provided as well. The uncertainties of the evolutionary ages due to inherent shortcomings in the models and due to the unclear effectiveness of diffusion are discussed. A first application to field single stars is presented.

Key words: Stars: evolution – stars: interior – stars: Population II

Send offprint requests to: A. Weiss; (e-mail address: aweiss@mpa-garching.mpg.de)
Correspondence to: A. Weiss

1. Introduction

The determination of stellar ages provides numerous clues on the evolution of the Milky May and its components. While the classical method for globular clusters relies on morphological features in the Hertzsprung–Russell-diagram (HRD), for example an age-dependent turn-off (TO) brightness, direct age determinations of individual stars is progressively becoming a feasible alternative. In this case, the age is obtained from the position of the star on an evolutionary track. Typical examples for this method are eclipsing binary systems such as AI Phe (Andersen et al. 1988; Milone et al. 1992) or ζ Aur (Bennett et al. 1996; Schröder et al. 1997), for which accurate masses and radii can be determined from the light-curves (photometry and spectroscopy needed), and the stellar composition is either assumed or obtained from spectral analysis. In this case, the requirement that both components should have the same age provides an independent test for stellar evolution theory. If the distance to a single star is known accurately (e.g. from HIPPARCOS parallaxes) and its composition, gravity and effective temperature can be determined spectroscopically, the same procedure can be applied as well. For example, this method has recently been used for metal-poor stars by Fuhrmann (1998; 2000) to deduce the formation history of bulge, thick and thin disk, and halo of the Milky Way. In the future, detached eclipsing binaries will hopefully be detected in globular clusters by massive photometric searches (e.g. in ω Cen, Kaluzny et al. 1996 and Kaluzny et al. 1997a, and in M4, Kaluzny et al. 1997b) and will then allow age determinations of individual cluster stars (Paczyński 1997).

To be prepared for this case, we provide a grid of evolutionary tracks for low-mass, metal-poor stars typical for Pop II. The grid not only extends over stellar mass (from $0.6 \cdots 1.3\,M_\odot$) but also over composition, both in metallicity Z and helium content Y. The latter parameter usually is kept at a fixed value (typically 0.23) or coupled to Z via an assumption about the chemical evolution. Due to the small absolute value of Z for Pop II stars, this is however an almost negligible effect. According to Paczyński (1997) it might be feasible to determine age *and* helium content of members of detached eclipsing binary systems and therefore calculations for different values of the initial helium abundance are necessary.

As a further effect microscopic diffusion has to be considered. Although it has become evident that it is operating in the Sun (Richard et al. 1996; Guenther & Demarque 1997), there are also arguments that diffusion may not be as efficient as calculated, as can be seen from the high abundance of ^{7}Li still present in the photosphere of metal-poor low-mass stars (Vauclair & Charbonnel 1998). Therefore, calculations with and without diffusion have been performed to cover the whole possible range.

In Sect. 2 we will summarize the main properties of our stellar evolution code and the calculations done. After this, the results will be presented. We make available tables with the full evolutionary properties of all cases calculated. These can be used for isochrone calculations as well, if needed. We avoid transformations into observed colours and magnitudes for several reasons: firstly, such transformations always involve a further source of uncertainty (see Weiss & Salaris 1999 for a discussion); secondly, they can, if needed, easily be applied, since the tables contain all necessary data; and finally, the data expected from the analysis of binary lightcurves and from spectroscopy will yield physical quantities, anyhow. To facilitate the derivation of the stellar age from given values of the global stellar properties, fitting formulae and the corresponding coefficients will be supplied as well. In Sect. 4 we will finally discuss the accuracy of such direct age determinations with special emphasis laid upon the comparison with other, independent work, because this will provide insight into the inherent systematic uncertainties of theoretical stellar evolution calculations. In the absence of suitable binary systems, we have applied our results to a few nearby single stars with known absolute parameters. This will be presented in Sect. 4 as well, before the conclusions close the paper.

2. The stellar evolution code

We are using the Garching stellar evolution code, which is a derivative of the original Kippenhahn-code (Kippenhahn et al. 1967) developed and improved over the years. While new properties of the code have always been documented in the corresponding publications, we summarize them here again for completeness:

Numerical aspects: The Lagrangian spatial grid (in relative mass M_r/M) adopts itself to structure changes. Its resolution is controlled by an algorithm ensuring that the partial differential equations are solved with a given accuracy (Wagenhuber & Weiss 1994). Since all composition changes are calculated between two models of two successive evolutionary ages, the evolution of temperature and density during this time-step has to be given at each grid-point. We use a predictor–corrector scheme for this (Schlattl 1996; Schlattl et al. 1997). The assumption of constant T and ρ can be used as an alternative, but requires time-steps smaller by about a factor of 2–5. Nuclear burning and particle transport processes (convection and diffusion) are calculated either simultaneously in a single iterative scheme with a generalized Henyey-solver (Schlattl 1999) or separately in a burning–mixing–burning–. . . sequence. In the latter case, the network solves the linearized particle abundance equations in an implicit way. In both cases a number of time-steps, which are smaller than that between the two models and which are adopting to composition changes, are followed until the whole evolutionary time-step is covered.

Opacities: We use as the sources for the Rosseland mean opacities the latest OPAL tables (Iglesias & Rogers 1996) and the molecular opacities by Alexander & Ferguson (1994). Both groups provided us (Rogers 1995, private communication, and Alexander, 1995, private communication) with tables for *exactly the same compositions* including the enhancement of α-elements (see Salaris & Weiss 1998 for details). The tables, which have a common T-ρ-grid, can smoothly be merged and together with electron conduction opacities (Itoh et al. 1983) result in consistent tables for all stellar interior conditions encountered. The interpolation within a single table is done by bi-rational two-dimensional splines (Spaeth 1973), which contain a free parameter allowing the transition from standard cubic to near-linear interpolation. This avoids unwanted spline oscillations but guarantees that the interpolant is always differentiable twice. We then interpolate in a 3x3 cube in X–Z–space to the grid-point's composition by two independent polynomial interpolations of degree 2. The cube of table compositions is chosen such that the central point is closest to the actual composition under consideration.

Equation of state: We use, where possible, the OPAL equation of state (Rogers et al. 1996) with the interpolation procedures provided by the same authors along with the EOS tables. For low densities and temperatures, we use our traditional Saha-type EOS for a partially ionized plasma or approximations for a degenerate electron gas (see Kippenhahn et al. 1967, Weiss 1987, Wagenhuber 1996 for details). However, we did not calculate models not being covered by the OPAL EOS for the larger part. This limits the mass range to $\geq 0.6\,M_\odot$.

Convection: Convection is treated in the standard mixing-length approach. No overshooting or semi-convection is considered. The mixing-length parameter is calibrated with a solar model calculated without diffusion; the resulting value for the physical input employed here is 1.59 pressure scale heights. Note that it would be slightly different for solar models including diffusion. Convective mixing is either assumed to be instantaneous or treated as a fast diffusive process in the case that all processes affecting the chemical composition are treated simultaneously.

Neutrino emission: Energy losses due to plasma processes are included according to Haft et al. (1994) for plasma-neutrinos and Munakata et al. (1985) for photo- and pair-neutrinos.

Nuclear reactions: We use the Caughlan & Fowler (1988) reaction rates and the Salpeter formula for weak screening. The nuclear network follows the evolution of ^{1}H, ^{3}He, ^{4}He, ^{12}C, ^{13}C, ^{14}N, ^{15}N, ^{16}O, ^{17}O. All other species in the *pp*-chain and CNO-cycles are assumed to be in equilibrium (this is justified because it assumes only that β-decays are faster than p-captures). The network can also treat later burning phases, but this is of no concern here because calculations were stopped at the onset of the core helium flash.

Diffusion: We consider the diffusion of hydrogen and helium. While our code also allows for metal diffusion, we ignored this here for reasons of CPU economy. Experience from solar models shows that the effect of metal diffusion on the interior evolution is only a fraction of that of H/He diffusion. This is confirmed by test calculations in which metal diffusion was included (see next section). The various coefficients of the particle diffusion equations are calculated according to Thoul et al. (1994) with the routine provided kindly by A. Thoul (1997, private communication). If diffusion is considered, it turned out to be both more accurate and numerically stable to treat diffusion and burning in a single numerical algorithm (see above).

3. Calculations and results

3.1. Details of the calculations

We have calculated two complete sets of models, one (canonical) without and one with particle diffusion (denoted "C" and "D"). In each set the following values of mass and composition were explored:

1. *Mass:* $M = 0.6 \cdots 1.3\,M_\odot$ in steps of $0.1\,M_\odot$
2. *Helium:* $Y = 0.20,\ 0.25,\ 0.30$
3. *Metallicity:* $Z = 0.0001,\ 0.0003,\ 0.001,\ 0.003$

Due to the varying helium abundance, [Fe/H] is not constant for fixed Z. Table 1 lists [Fe/H] for all mixtures.

Table 1. [Fe/H] for the twelve initial compositions, for which evolutionary tracks have been computed.

$\downarrow Y \mid Z \rightarrow$	0.0001	0.0003	0.0010	0.0030
0.20	-2.645	-2.168	-1.644	-1.166
0.25	-2.617	-2.140	-1.616	-1.138
0.30	-2.587	-2.110	-1.586	-1.108

The metallicity range is that for typical globular clusters, but is not covering the most metal-rich ones like 47 Tuc or M107. The same enhancement of α-elements (Salaris & Weiss 1998) is always assumed and is the one for which we have the opacity tables available. Z therefore denotes the total metallicity including the α-element enhancement in all cases. Because α-element enhancement is typical for Pop II stars, no calculation for solar metal ratios has been done. We recall that for very low metallicities, the evolution depends primarily on the total metallicity (Salaris et al. 1993) and only slightly on the internal metal distribution. This, however, becomes non-negligible at the upper end of our metallicity range. For example, Salaris & Weiss (1998) find that already at $Z = 0.002$ the turn-off of isochrones is about 0.05 mag brighter for models which include α-enhancment as compared to a solar-scaled mixture with identical Z. Also, the RGB colour is bluer by ≈ 0.05 mag.

It is not yet clear whether the amount of oxygen enhancement in metal-poor stars is independent of metallicity (see Gratton et al. 2000 for a recent result), or whether there are systematic variations of [O/Fe] with [Fe/H] (see Israelian et al. 1998 for unevolved metal-poor stars). In both cases, the oxygen enhancement of our metal mixture ([O/Fe] = 0.5) is a good representation of the average enhancement in the metallicity range under consideration. The same is true for the magnesium overabundance (Fuhrmann 1998; see also Salaris & Weiss 1998 for the spread of abundances of other α-elements). Variations around the mean α-enhancement are a second-order effect, which could be considered only in modeling individual objects, provided the availability of appropriate opacity tables.

The helium values of our mixtures were chosen as to certainly cover the possible range, with the central value of $Y = 0.25$ being close to a primordial value of 0.244 ± 0.002 (Izotov & Thuan 1998). This value is somewhat higher than the traditionally assumed 0.23, which, however is too low, even for the more generally accepted primordial value of 0.234 ± 0.002 (Olive et al. 1997). Different initial helium contents in the calculations allow save interpolation to any prefered value or to keep it as a free parameter. Some additional mixtures were considered for specific mass values in order to be able to compare with published results (see Sect. 4.1).

All calculations were started from homogeneous zero-age main-sequence (ZAMS) models with vanishing gravothermal energies. This implies adjustment of isotopes to their equilibrium values in the stellar core; this period lasts for several 10^7 years. The resulting small loop in the HRD is omitted in all figures and tables and the ages reset to zero for the models with minimum gravothermal energy production. This definition does not necessarily coincide with the minimum luminosity during the initial loop, which would be an alternative choice for the ZAMS position. For the lower masses our definition corresponds to ages of a few 10^7 yrs, for the higher masses to about 10^5 yrs or even less. The evolution is followed up to the tip of the red giant branch (RGB), when helium violently ignites in an off-center shell (core helium flash). No shell-shifting or other approximation is done on the RGB; the full evolution is followed. Typically, the calculations need about 200 time-steps until core hydrogen exhaustion, another 300 until the onset of the first dredge-up, 700 to the end of it and a further 8000 to the tip of the RGB.

The spatial resolution of the models is such that on the main sequence of order 600 and on the RGB twice as many grid-points are needed. We verified that increasing the number of grid-points and time-steps does not influence the relation between luminosity and age by more than a per cent.

3.2. Evolutionary tracks

We display in Fig. 1 the evolution without diffusion ("C"-set) of all masses for the case which is close to the centre of our 3x4 composition space, i.e. for $(Y, Z) = (0.25, 0.0003)$, and in Fig. 2 the changes of the evolution due to variations of the composition for the case of the $0.8\,M_\odot$ model. The left panels show the HRD-tracks (top: varying helium content; bottom: varying metallicity) and the right ones the evolutionary speed. The well-known effects, such as a lower effective temperature for higher Z or lower Y or shorter main-sequence (MS) lifetimes for higher Y or lower Z, are recognizable.

The influence of diffusion both on the track in the HRD and on the evolutionary speed is displayed in Fig. 3 for the same reference composition. For sake of clarity the evolution of only a few selected masses are shown. The effects – for example, lower effective temperature and brightness during the main sequence – are as known from other investigations (e.g. Cassisi et al. 1998). MS-lifetimes get shorter due to the diffusion of helium into the center, which is effectively equivalent to a faster aging of the star. For given MS-luminosity, TO-models with diffusion can be younger by up to 1 Gyr compared to those calculated canonically. We recall that we include only H/He-diffusion in the grid

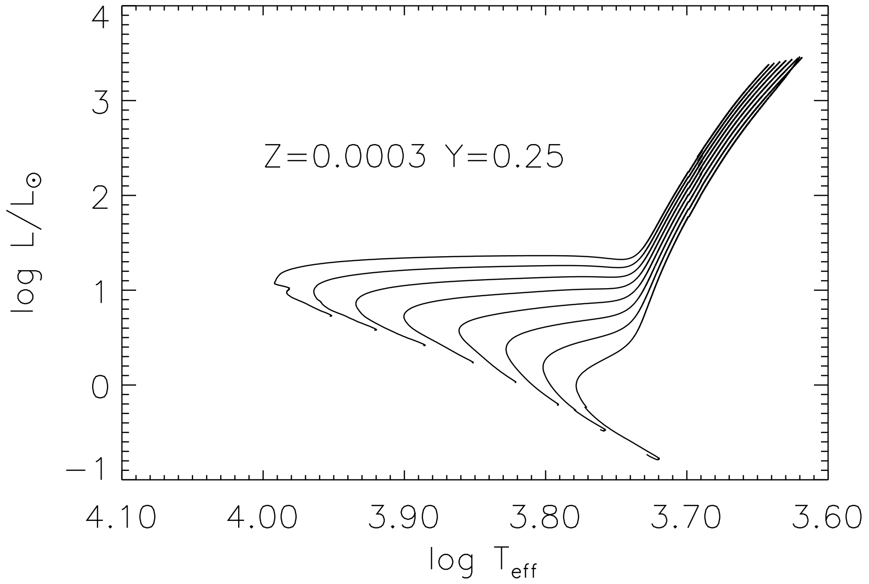

Fig. 1. Evolution (without diffusion) in the HRD for all masses (0.6, 0.7, . . . 1.3 $M_\odot$) with composition $Y = 0.25$, $Z = 3 \cdot 10^{-4}$

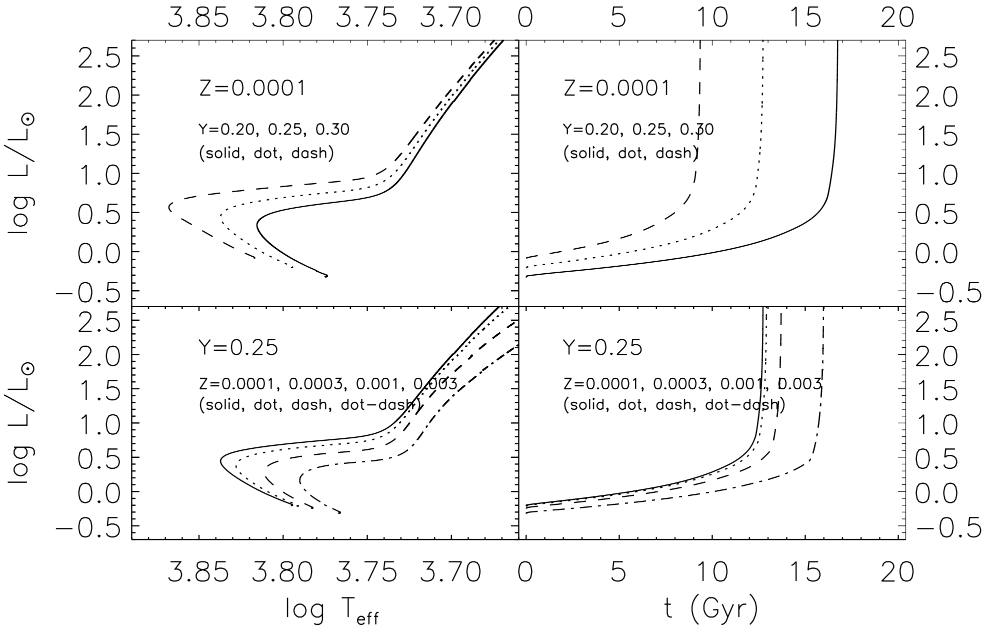

Fig. 2. Influence of composition changes on the evolution of the $0.8\,M_\odot$ model (no diffusion)

of models of this paper. To verify that the additional metal diffusion has a negligible influence on the evolutionary tracks and in particular on lifetimes, we show in Fig. 4 the comparison between models with H/He- and H/He/Z-diffusion in the case of mixture $(Y, Z) = (0.25, 0.001)$. We chose a higher metallicity than in the previous example because the depletion of the stellar envelopes in metals due to diffusion is expected to have a higher effect for higher initial metallicity. As Fig. 4 demonstrates, the age-luminosity relation is almost identical and the track in the HRD only slightly shifted to the blue

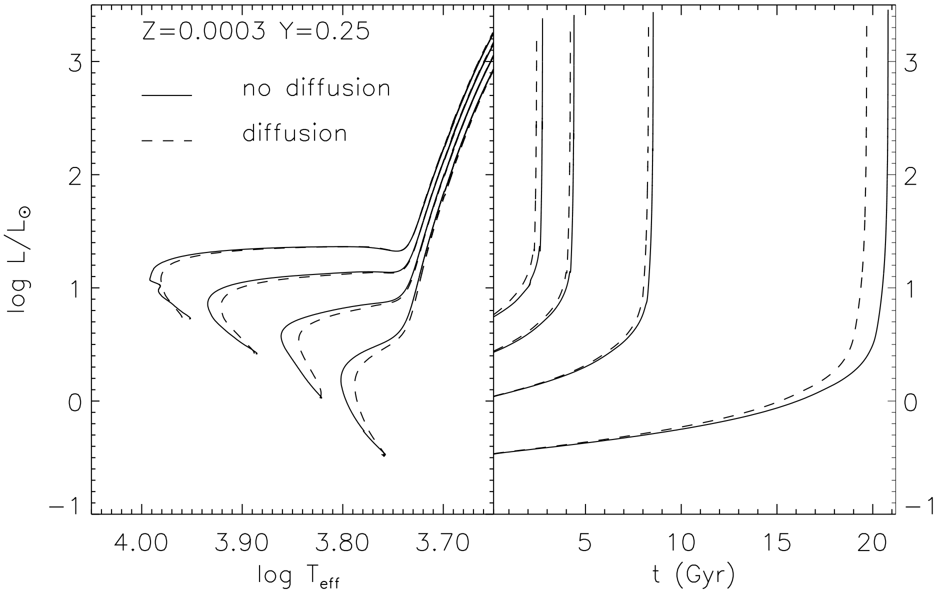

Fig. 3. Influence of diffusion on the evolutionary tracks (left panel) and lifetimes (right panel) for selected masses (0.7, 0.9, 1.1, 1.3 $M_\odot$) and the same composition as in Fig. 1

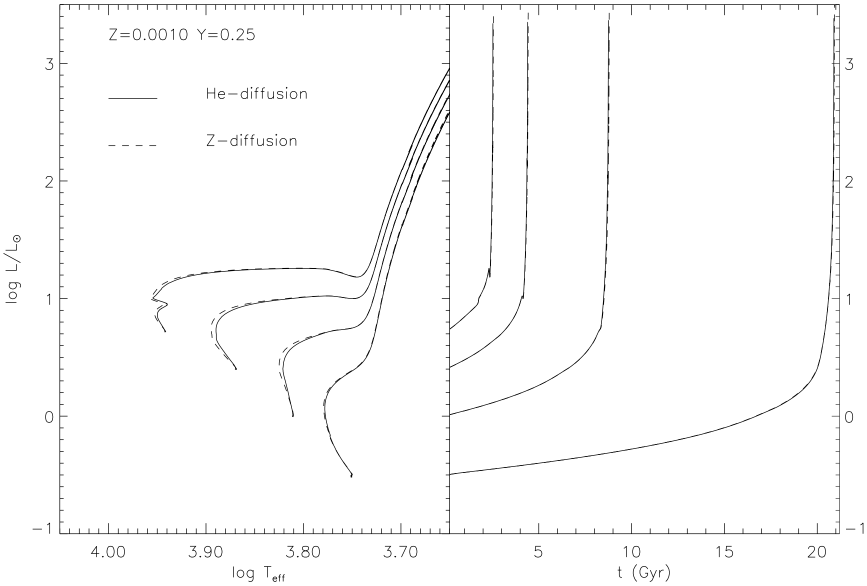

Fig. 4. Influence of metal diffusion on the evolutionary tracks (left panel) and lifetimes (right panel) for composition (Y, Z) = (0.25, 0.001) and the same selected masses composition as in Fig. 3. Comparison is made with the case of hydrogen-helium diffusion

because of the decrease in surface metallicty. After the turn-off, the deepening convective envelope is mixing back quickly the diffused elements such that the initial envelope composition is almost restored (cf. Salaris et al. 2000). The tracks approach each other therefore during the subgiant evolution. The surface metallicity drops to a minimum of 42% of the initial one for the $M/M_\odot = 0.8$ model, which is good agreement with results by Salaris et al. (2000).

The evolutionary properties for *all* cases calculated are given in tables in Appendix A.

3.3. Age-luminosity relations

It would be desirable to have an analytical formula $t(L, M, Y, Z)$, which returns the age of a star for any given set of observed quantities. However, there is no simple analytical fit to the results of the evolutionary calculations and high-order fitting formulae are not practical. We have attempted to provide fits which are a compromise between accuracy and simplicity and start with providing a fitting formula to obtain $t(L)$ for each individual mass calculated. This formula is

$$t[10^{10}\ \mathrm{yr}] = a - \exp(-(\log(L/L_\odot) + b) \cdot c) \tag{1}$$

and in general fits the evolutionary ages after the initial 100-200 Myr with an accuracy of a few percent. The coefficients a, b and c depend on mass and composition. Tables 2 and 3 contain the values of all of them for all cases. To illustrate the fit quality, both the fit and the relative fitting accuracy are shown for two selected cases in Figs. 5 and 6 (solid vs. dotted lines).

Table 2. Parameters for the function $t = a - \exp(-(\log(L/L_\odot) + b) \cdot c)$. t is in 10^{10} years. For each combination of mass $M/M_\odot$, metallicity Z and helium content Y the fitting parameters a, b and c are given. Case "C" (no diffusion).

$M/M_\odot$	Z	$Y = 0.20$			$Y = 0.25$			$Y = 0.30$		
		a	b	c	a	b	c	a	b	c
0.60	0.0001	4.68683	0.35586	3.05625	3.53605	0.34283	3.02336	2.60818	0.33038	3.02014
	0.0003	4.77712	0.36200	3.06499	3.59575	0.34984	3.05363	2.65045	0.33699	3.05964
	0.0010	5.10040	0.37619	3.07399	3.82210	0.36438	3.09124	2.81103	0.35093	3.11996
	0.0030	6.06607	0.37026	2.94939	4.52971	0.38835	3.13366	3.24782	0.37750	3.16778
0.70	0.0001	2.75644	0.23948	3.07744	2.04816	0.22465	3.11651	1.50112	0.20670	3.16830
	0.0003	2.80616	0.24708	3.12424	2.08362	0.23132	3.17035	1.52506	0.21224	3.22277
	0.0010	2.98995	0.26352	3.19686	2.21790	0.24602	3.25090	1.61912	0.22531	3.30198
	0.0030	3.49486	0.29429	3.25585	2.58532	0.27583	3.33550	1.88109	0.25322	3.39598
0.80	0.0001	1.68343	0.13525	3.22279	1.27581	0.11091	3.25539	0.93729	0.08773	3.30100
	0.0003	1.74860	0.13805	3.27157	1.29541	0.11599	3.31912	0.94964	0.09107	3.37295
	0.0010	1.86228	0.15350	3.37035	1.37588	0.12939	3.40681	1.00329	0.10161	3.46594
	0.0030	2.18269	0.18574	3.48119	1.60682	0.15929	3.52297	1.16197	0.12978	3.56537
0.90	0.0001	1.13503	0.02607	3.34182	0.84599	0.00074	3.38876	0.62575	-0.02647	3.43726
	0.0003	1.15214	0.03091	3.41167	0.85656	0.00347	3.47214	0.63156	-0.02646	3.53322
	0.0010	1.22304	0.04434	3.51816	0.90404	0.01403	3.58107	0.66144	-0.02009	3.66277
	0.0030	1.43144	0.07579	3.65932	1.04797	0.04264	3.71174	0.75716	0.00348	3.81259
1.00	0.0001	0.78944	-0.07630	3.47280	0.59243	-0.10569	3.53159	0.44517	-0.13915	3.61112
	0.0003	0.79898	-0.07378	3.56344	0.59726	-0.10614	3.64016	0.44737	-0.14257	3.73657
	0.0010	0.84194	-0.06398	3.70478	0.62523	-0.10057	3.79452	0.46323	-0.14090	3.91179
	0.0030	0.97527	-0.03456	3.87128	0.71489	-0.07726	3.99567	0.51923	-0.12586	4.15912
1.10	0.0001	0.57401	-0.17656	3.62913	0.44051	-0.21321	3.73425	0.34106	-0.26244	3.91988
	0.0003	0.57955	-0.17673	3.74518	0.44161	-0.21628	3.87160	0.34008	-0.26682	4.06653
	0.0010	0.60410	-0.17304	3.95072	0.45619	-0.21517	4.07949	0.34790	-0.27014	4.34218
	0.0030	0.69070	-0.14894	4.19878	0.50901	-0.19791	4.33119	0.37785	-0.25579	4.66150
1.20	0.0001	0.44274	-0.27904	3.85851	0.34658	-0.32992	4.05838	0.26632	-0.38467	4.26117
	0.0003	0.44597	-0.28260	4.01666	0.34535	-0.33435	4.22578	0.26563	-0.40273	4.59135
	0.0010	0.45712	-0.28112	4.25898	0.35288	-0.33823	4.54620	0.27248	-0.42019	5.10977
	0.0030	0.50782	-0.26315	4.55547	0.38208	-0.32214	4.91328	0.28638	-0.40417	5.49256
1.30	0.0001	0.35440	-0.38785	4.17826	0.27521	-0.44247	4.38679	0.21011	-0.50132	4.62344
	0.0003	0.35614	-0.39527	4.39311	0.27396	-0.45857	4.71954	0.21034	-0.53311	5.13498
	0.0010	0.36100	-0.39740	4.74103	0.28144	-0.47611	5.28857	0.21569	-0.55507	5.76582
	0.0030	0.39037	-0.38075	5.16706	0.29669	-0.46093	5.76533	0.22379	-0.52555	5.86558

As a next step, we tried to model the dependence of the fitting coefficients in Eq. (1) on mass. Globally, $a(M)$ and $c(M)$ appear to be reminiscent of a parabolic function,

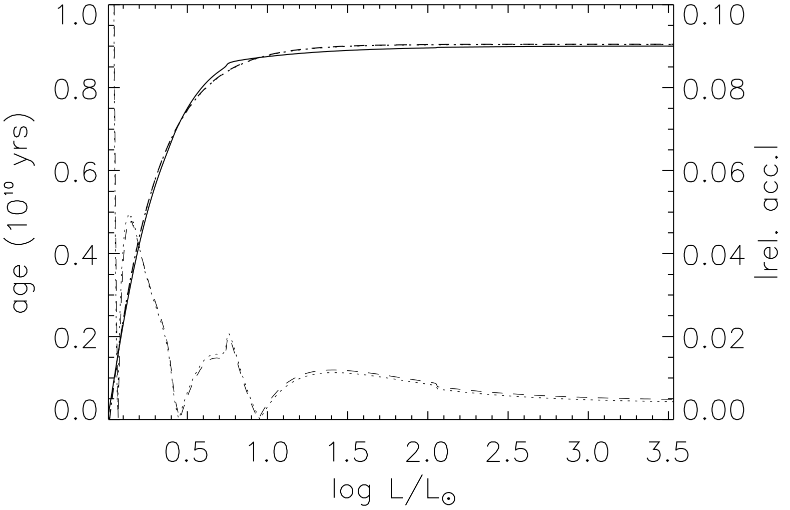

Fig. 5. $t(\log L)$ (left axis) from the calculation of a (case C) model with $M/M_\odot = 0.90$, $Y = 0.25$, $Z = 0.001$ (solid) and as obtained from Eq. (1) (dotted) or Eq. (2) (dashed). The relative accuracy (absolute value) for both fitting functions is also shown (corresponding thin lines; right axis)

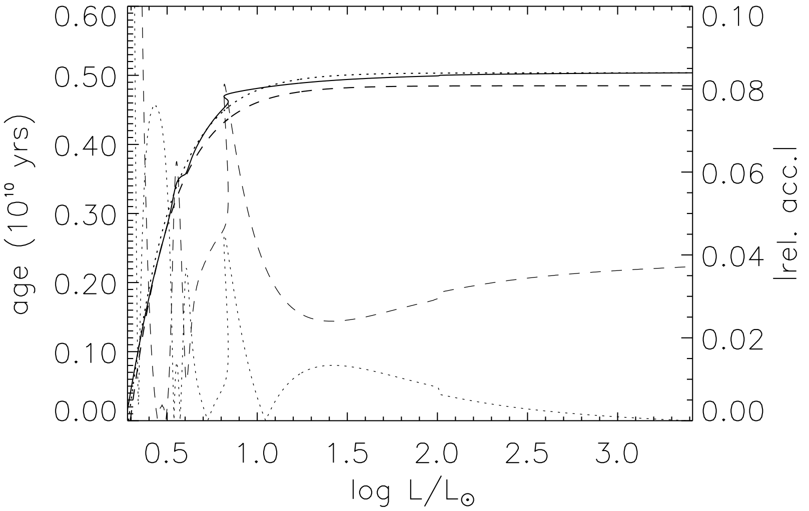

Fig. 6. As Fig. 5, but for a model with diffusion (case D) and $M/M_\odot = 1.00$, $Y = 0.30$, $Z = 0.003$

while $b(M)$ is close to a linear one. However, individual coefficient values lie off the main trend, such that higher order fits are required. We used the cubic polynomial

$$a = a_0 + a_1 \cdot (M/M_\odot) + a_2 \cdot (M/M_\odot)^2 + a_3 \cdot (M/M_\odot)^3 \qquad (2)$$

(and equivalent expressions for b and c). The individual coefficients still depend on Y and Z. We found that with this approximation the coefficients could be modelled again with an accuracy of a few percent. The coefficients $a_0 \dots c_3$ are listed for both sets of calculations in Tables 4 and 5. The fits obtained by using Eq. (2) with the coefficients taken from Tabs. 4 and 5 and inserting the proper mass value to obtain the coefficients of Eq. (1) are shown in Figs. 5 and 6 (dashed lines) as well. While in the former case the fit quality is not degraded, it is worse in the latter one, but the errors remain within 5% for most of the evolution (see the thin dashed line), except for the very end of the main-sequence, where the luminosity of the more massive stars shows the complicated "kink"-behaviour in the HRD, which cannot be modelled by this fitting function.

Table 3. As Table 2, but for case "D" (with diffusion).

$M/M_\odot$	Z	$Y = 0.20$			$Y = 0.25$			$Y = 0.30$		
		a	b	c	a	b	c	a	b	c
0.60	0.0001	4.32887	0.37567	3.02190	3.26232	0.36413	2.99265	2.41195	0.35193	2.99435
	0.0003	4.40146	0.38369	3.04085	3.31250	0.37205	3.02861	2.44809	0.35903	3.03903
	0.0010	4.68208	0.40064	3.06122	3.50928	0.38869	3.07645	2.58894	0.37435	3.10479
	0.0030	5.49931	0.40621	2.96719	4.04219	0.41951	3.11132	2.96640	0.40530	3.16241
0.70	0.0001	2.60728	0.25458	3.07649	1.93855	0.23953	3.11674	1.42432	0.22087	3.16418
	0.0003	2.65059	0.26277	3.12750	1.97077	0.24646	3.16889	1.44621	0.22648	3.22177
	0.0010	2.82116	0.28025	3.20341	2.09415	0.26202	3.25551	1.53329	0.24023	3.30384
	0.0030	3.27308	0.31450	3.26899	2.42215	0.29481	3.34407	1.76776	0.27068	3.41326
0.80	0.0001	1.64775	0.14155	3.22820	1.22635	0.12050	3.26636	0.90293	0.09644	3.31164
	0.0003	1.67685	0.14833	3.28972	1.24557	0.12581	3.32984	0.91498	0.09989	3.38364
	0.0010	1.78747	0.16442	3.38334	1.32252	0.13983	3.41672	0.96556	0.11174	3.47145
	0.0030	2.11192	0.18609	3.33429	1.53360	0.17155	3.54847	1.11111	0.14061	3.58888
0.90	0.0001	1.10076	0.03244	3.36031	0.82064	0.00676	3.40366	0.60561	-0.02245	3.46209
	0.0003	1.11760	0.03745	3.43144	0.83141	0.00965	3.48631	0.61216	-0.02207	3.55489
	0.0010	1.18750	0.05159	3.53355	0.87804	0.02080	3.59323	0.64233	-0.01466	3.68069
	0.0030	1.38137	0.08447	3.66996	1.01169	0.05043	3.73441	0.73241	0.01050	3.82981
1.00	0.0001	0.76908	-0.07288	3.49792	0.57533	-0.10408	3.56717	0.42600	-0.13838	3.63774
	0.0003	0.77900	-0.07044	3.59247	0.58121	-0.10383	3.66964	0.42929	-0.14256	3.77247
	0.0010	0.82251	-0.05927	3.72051	0.61003	-0.09704	3.81815	0.44773	-0.14085	3.95451
	0.0030	0.94850	-0.02913	3.89619	0.69552	-0.07280	4.02281	0.50360	-0.12202	4.19106
1.10	0.0001	0.55857	-0.17708	3.67657	0.41930	-0.21320	3.75835	0.31158	-0.25374	3.86183
	0.0003	0.56415	-0.17722	3.79350	0.42210	-0.21775	3.91291	0.31300	-0.26297	4.04566
	0.0010	0.59210	-0.17067	3.97315	0.44043	-0.21741	4.13788	0.32390	-0.26772	4.30476
	0.0030	0.67508	-0.14611	4.22927	0.49579	-0.19793	4.40999	0.36014	-0.26203	4.79190
1.20	0.0001	0.41916	-0.28013	3.88606	0.31552	-0.32160	3.99623	0.23514	-0.36652	4.11702
	0.0003	0.42181	-0.28496	4.05931	0.31673	-0.33159	4.20871	0.23532	-0.38079	4.35825
	0.0010	0.43987	-0.28553	4.33719	0.32785	-0.33961	4.54623	0.24104	-0.39874	4.84120
	0.0030	0.49553	-0.26471	4.64456	0.36493	-0.33050	5.06159	0.26657	-0.40618	5.60667
1.30	0.0001	0.32287	-0.38193	4.13115	0.24368	-0.42705	4.25755	0.18201	-0.47279	4.36969
	0.0003	0.32393	-0.39226	4.37277	0.24378	-0.44282	4.53974	0.17950	-0.49064	4.69556
	0.0010	0.33549	-0.39965	4.75053	0.24998	-0.45894	5.04221	0.18393	-0.50652	5.21632
	0.0030	0.37394	-0.39030	5.34027	0.27690	-0.46505	5.89274	0.20304	-0.51820	6.03615

It is not useful to continue with finding fitting functions in composition, because we have only a 3x4 composition space and such functions would require at least 3 parameters for each dimension. Further fitting would therefore only increase the total number of coefficients. Rather, we recommend to interpolate between the ages obtained through Eqs. (2) and (1) to the composition of any observed star.

Table 4. Fitting the mass-dependence of the coefficients of Table 2. The three lines of each composition correspond to the three parameters a, b, and c; for example, the first lines contain coefficients a_0, a_1, a_2, and a_3 of Eq. (2).

Y	Z	a, b, c			
0.20	0.0001	29.2077	-70.7155	58.7312	-16.4698
		1.4060	-2.4031	1.3708	-0.4489
		0.1911	9.0341	-9.6597	3.8994
0.20	0.0003	29.7043	-71.7262	59.3967	-16.6087
		1.3975	-2.3636	1.3456	-0.4525
		-0.2651	10.6190	-11.4234	4.6238
0.20	0.0010	31.4324	-75.6675	62.4585	-17.4163
		1.3120	-2.0165	0.9768	-0.3362
		-1.5348	14.8288	-15.9140	6.3227
0.20	0.0030	36.8363	-88.4998	72.8976	-20.2998
		0.8201	-0.4514	-0.5362	0.1330
		-4.3950	23.6936	-24.8876	9.4754
0.25	0.0001	22.5447	-55.0764	46.1447	-13.0444
		1.1258	-1.5493	0.4975	-0.1800
		2.7059	1.1295	-1.7242	1.4248
0.25	0.0003	22.8452	-55.7195	46.5951	-13.1477
		1.4040	-2.4222	1.4181	-0.5054
		-1.0202	13.5479	-15.1164	6.2240
0.25	0.0010	24.0297	-58.3325	48.5215	-13.6191
		1.6165	-3.0661	2.1179	-0.7673
		-4.8060	26.6803	-29.9153	11.8184
0.25	0.0030	27.9680	-67.6242	55.9981	-15.6582
		1.4430	-2.3857	1.3930	-0.5264
		-4.6154	26.4036	-29.9896	12.1702
0.30	0.0001	16.8533	-41.4895	35.0619	-9.9976
		0.8082	-0.5057	-0.6429	0.1976
		4.7946	-5.7016	5.4242	-0.8754
0.30	0.0003	17.0790	-41.9770	35.3982	-10.0704
		0.9524	-1.0040	-0.0459	-0.0471
		3.5676	-0.6182	-1.2110	2.0137
0.30	0.0010	18.1267	-44.4785	37.4060	-10.6092
		0.7120	-0.1966	-0.8545	0.1964
		7.8855	-13.4807	10.8945	-1.3620
0.30	0.0030	20.4666	-49.7150	41.3637	-11.6164
		0.3008	1.3422	-2.5921	0.8232
		20.2151	-54.5229	55.3097	-16.8058

Table 5. As Tab. 4, but the case D coefficients of Tab. 3

Y	Z	a, b, c			
0.20	0.0001	26.4015	-63.2538	52.1585	-14.5656
		1.2280	-1.6948	0.5350	-0.1415
		2.1368	2.1647	-1.8484	1.0488
0.20	0.0003	26.7886	-64.1169	52.8122	-14.7334
		1.2478	-1.7368	0.5949	-0.1764
		1.6609	3.9792	-4.0180	1.9709
0.20	0.0010	28.3804	-67.7799	55.6983	-15.5053
		1.2038	-1.5540	0.4377	-0.1471
		1.7792	4.1186	-4.7200	2.5472
0.20	0.0030	32.9185	-78.2930	64.0441	-17.7525
		1.1598	-1.4451	0.4589	-0.2035
		-4.9779	25.6408	-27.2815	10.5084
0.25	0.0001	19.9386	-47.9299	39.6462	-11.1021
		1.1975	-1.5798	0.3577	-0.0798
		2.2408	1.7358	-1.2970	0.8889
0.25	0.0003	20.2355	-48.6066	40.1675	-11.2377
		1.1670	-1.4564	0.2420	-0.0571
		2.5421	1.0307	-0.8450	0.9498
0.25	0.0010	21.4126	-51.3506	42.3545	-11.8293
		1.0981	-1.1875	-0.0110	0.0024
		2.0184	3.4628	-4.2511	2.5979
0.25	0.0030	24.4112	-58.2151	47.7292	-13.2546
		1.2151	-1.5061	0.3984	-0.1801
		-1.2354	15.6116	-18.9391	8.5766
0.30	0.0001	14.7503	-35.5174	29.4317	-8.2556
		1.0895	-1.2037	-0.1142	0.0889
		3.4016	-2.1258	2.9171	-0.5447
0.30	0.0003	15.0295	-36.2278	30.0487	-8.4381
		1.0026	-0.8747	-0.4748	0.2030
		3.2613	-1.4881	2.0549	-0.0469
0.30	0.0010	15.8313	-38.0600	31.4652	-8.8065
		0.5327	0.7118	-2.1346	0.7475
		9.0922	-19.5958	20.0909	-5.6196
0.30	0.0030	18.0913	-43.3256	35.6464	-9.9272
		0.0508	2.3708	-3.8357	1.2883
		20.6253	-56.0962	57.0595	-17.3318

4. Discussion

4.1. Comparison with other theoretical results

Paczyński (1997) has argued that the achievable accuracy in the observations of detached eclipsing binaries in globular clusters translates into an accuracy of the determined stellar age of order 2%. Very justified, Paczyński states that "the uncertainties in the stellar models are certainly larger than that". To give an impression of how large these uncertainties might be, we compare our results to some other contemporary calculations of comparable models.

In a first step we compare ZAMS positions. Tout et al. (1996) have given analytic functions for ZAMS-positions as function of mass and metallicity based on their own calculations. Since they used a fixed Y-Z-relation we cannot straightforwardly compare their results with our low-metallicity models. The composition closest to their relation is that with $Y = 0.25$ and $Z = 0.0010$, which is to be compared with $Y = 0.2420$ (and the same Z). We find that over the mass range of our calculations our ZAMS models are 0.04 dex brighter in L (with very small variation) and slightly hotter (0.04 dex in $T_{\rm eff}$ for the lowest masses to 0.01 dex for the highest ones). Both effects are consistent with the higher helium content of our models and the fact that we are using a more up-to-date EOS. For a solar-like mixture ($Y = 0.28$, $Z = 0.02$), for which we made additional calculations, the differences are below the 0.02 dex level, reflecting the EOS-change only. We have also calculated a set of ZAMS models for all three metallicities and the same helium content as in Tout et al. (1996), but using our old EOS. In this case differences are below 0.01 dex both in luminosities and effective temperatures with no systematic effect recognizable.

Table 6. Comparison between our models and those of Baraffe et al. (1997) with $Z = 0.0002$ (upper group) and 0.001 (lower group). The first line in each case (0.7 and 0.8 $M/M_\odot$) gives the Baraffe et al. (1997) data at 10 Gyr, the second and third line our results for the two bracketing metallicities resp. the second line our corresponding model. The comparison is made at same age (colums 2 and 3) or at same luminosity (columns 4 and 5; age in Gyr). All models have $Y = 0.25$.

M/Z	$\lg T_{\rm eff}$	$\log L/L_\odot$	$\lg T_{\rm eff}$	age
$M/M_\odot = 0.8$	3.825	0.334		
$Z = 0.0001$	3.832	0.285	3.835	10.4
$Z = 0.0003$	3.825	0.255	3.828	10.8
$M/M_\odot = 0.7$	3.772	-0.265		
$Z = 0.0001$	3.784	-0.233	3.781	8.8
$Z = 0.0003$	3.780	-0.250	3.779	9.4
$M/M_\odot = 0.8$	3.800	0.199		
$Z = 0.001$	3.809	0.165	3.810	10.4
$M/M_\odot = 0.7$	3.755	-0.326		
$Z = 0.001$	3.771	-0.298	3.768	8.8

Next, we compared with results by Baraffe et al. (1997), where the most important difference to our calculations is the use of the Saumon-Chabrier EOS (Saumon et al. 1995). Baraffe et al. (1997) list data for a set of models with $Y = 0.25$ and metallicities of $Z = 0.001$ and 0.0002, the latter one being intermediate between the lower two of our values. The age of these models is 10 Gyr. Table 6 shows how our models compare either at the same age or for the same luminosity. Comparing at the same age, our models are less luminous by about 0.06 dex for $M/M_\odot = 0.8$ but brighter by about 0.02 dex for $M/M_\odot = 0.7$. This translates into age differences (if comparison at identical luminosity is made) of about +0.5 resp. −1.0 Gyr for both metallicities. Baraffe et al. (1997) used solar metal ratios, but at these low absolute metallicities there is almost no influence of the internal metal composition (solar or α-enhanced) as verified by Baraffe et al. (1997) themselves (see also Salaris & Weiss 1998).

Table 7. Comparison between turn-off data for our models and those of Cassisi et al. (1998; their Tab. 2) and Girardi et al. (1999). All models have $Y = 0.23$.

Z	$M/M_\odot$	age	$\log L/L_\odot$	$\lg T_{\rm eff}$	age	$\log L/L_\odot$	$\lg T_{\rm eff}$	age	$\log L/L_\odot$	$\lg T_{\rm eff}$
		Cassisi et al. (1998)			Girardi et al. (1999)			this paper		
0.0001	0.80	11.6	0.410	3.826				12.2	0.415	3.829
0.0002	0.80	11.2	0.378	3.824				12.1	0.380	3.824
0.0010	0.70	20.0	0.060	3.777	21.6	0.074	3.784	21.8	0.074	3.783
0.0010	0.80	11.7	0.231	3.799	12.4	0.240	3.807	12.4	0.249	3.805
0.0010	0.90	7.4	0.393	3.822	7.6	0.406	3.829	7.7	0.394	3.828
0.0010	1.00	5.0	0.577	3.852	5.0	0.567	3.855	5.5	0.586	3.857

As a further test, we compared with results obtained with the FRANEC code, in particular those by Cassisi et al. (1998), who provide results for several combinations of input physics data. Their case-8 models are very similar to ours with the major exception being the treatment of the EOS outside the OPAL-range. We compare turn-off (TO) data for several cases in Tab. 7. The helium content is 0.23 for all models; we have made additional calculations with the same metallicity for this purpose. They were done without an explicit network (equilibrium abundances for the participating nuclei assumed). An explicit network increases the TO-age of the $0.8\,M/M_\odot$ model ($Z = 0.001$) by 0.5 Gyr; the inclusion of both network and pre-main sequence phase results in an increase of only 0.3 Gyr. We add that the calculations of Salaris & Weiss (1998), done with a variant of the FRANEC code, produce practically the same results as those by Cassisi et al. (1998); the small differences can be traced back mainly to the slightly higher helium content of 0.233 (at $Z = 0.001$). Overall, our models take longer to finish the MS-phase, with the differences getting smaller for higher metallicity and mass. With one exception, TO-ages are larger by less than 1 Gyr, or 5-10%. The comparison has been extended for RGB-tip data recently by Castellani et al. (2000), finding similar agreement. In the same table, for the highest metallicity, data from the latest Padua-tracks (Girardi et al. 1999) are listed as well. In this case, the agreement with our own results is even better.

We close this part with a few remarks on comparing isochrones with those by D'Antona et al. (1997; Tab. 2), who provide turn-off data for a large number of metallicities. At $Z = 0.0002$ and $Y = 0.23$, for which we again have made separate calculations, our 12 Gyr isochrone's TO is at $\log L/L_\odot = 0.469$ and $\log T_{\rm eff} = 3.829$, which is 0.021 dex brighter and 0.03 dex hotter than the corresponding one by D'Antona et al. (1997) (for mixing-length theory convection). The turn-off mass of $0.820 M_\odot$ is larger by $0.012 M_\odot$. For $Z = 0.001$, the differences are very similar ($\delta \log L/L_\odot = 0.031$ and a TO-mass higher by $0.018 M_\odot$). In fact, our TO-values are very close to those of the 11 Gyr isochrone of D'Antona et al. (1997). Part of the difference can be ascribed to different helium abundances, which is $Y = 0.235$ for their models in this case. A similar comparison with the Salaris & Weiss (1998) isochrones (for $Y = 0.233$ and $Z = 0.001$) gave an almost identical result: while at 9 Gyr our isochrone is very close to their corresponding one, the TO-brightness of our 13 Gyr isochrone is almost coincident with the 12 Gyr one of Salaris & Weiss (1998). This result is naturally to be expected from the comparison of Tab. 7. To conclude, it appears that the different low-mass star calculations agree with each other rather well, but the remaining differences, which are partly due to physical assumptions and partly due to technical details translate into age differences of up to 10% for any given composition, mass and luminosity. This can be viewed as the inherent uncertainty the evolutionary calculations carry with them.

4.2. A test application

The intended application of our tracks are detached eclipsing binary systems in globular clusters, which have been detected mainly by the OGLE team in several clusters (Kaluzny et al. 1996; Kaluzny et al. 1997a). Presently, for none of them follow-up spectroscopy needed to determine absolute parameters, has been concluded, although for one system in ω Cen preliminary data have been obtained (Kaluzny, private communication). Neither is there any other suitable system from another source available. All well-known systems, e.g. CM Dra and YY Gem (Chabrier & Baraffe 1995), μ Cas (Lebreton et al. 1999), or Gl570BC (Forveille et al. 1999), are too metal-rich ([Fe/H] > -0.76). We therefore turned to appropriate single stars to apply our relations and tracks. Fuhrmann (1998) provides a list of nearby disk and halo stars for which absolute parameters have been derived from a careful spectroscopic analysis in conjunction with Hipparcos parallaxes. From this list we have selected the five most metal-poor stars, of which two, however, are slightly beyond the upper boundary of our metallicity range (Tab. 8). All stars are enriched in Mg ($0.28 \leq$ [Mg/Fe] ≤ 0.46) and therefore are assumed to be α-enriched in agreement with our model compositions. Errors in [Fe/H] and $M_{\rm bol}$ are given in Tab. 8 as well, and are usually very small. The largest uncertainty comes from the mass, which Fuhrmann (1998) estimates to be of order 5%, or generally, less than 10%. The uncertainty in $T_{\rm eff}$ is ± 80 K in all cases. Fuhrmann (1998) classifies 4 of the selected stars as halo stars, and the fifth one (HD201891) as belonging to the thick disk.

If atomic diffusion is in operation, the presently observed and spectroscopically determined metallicity depends on both the initial one and on age. While in globular clusters the initial metallicity of main-sequence and turn-off stars can be estimated quite accurately from that of cluster giants (Salaris et al. 2000), this is not possible for field stars. The degeneracy mentioned therefore does not allow to determine the age independently of some assumptions about the initial metallicity. We therefore applied only our $t(L)$-fitting formulae Eq. (1) and (2) without diffusion (case C) to these objects.

Table 8 contains age estimates in three steps: Column 6 gives the age derived from the models with $Y = 0.25$ and a metallicity closest to the determined one (column 2), i.e. without any interpolation in [Fe/H] (cf. Tab. 1). In column 8, the age obtained from interpolation to the observed [Fe/H] (but the same helium content) is listed, and in column 10 that resulting from interpolation to $Y = 0.235$ (the "generic" Pop II helium abundance).

Table 8. Application of Eq. 2 (for the "C"-case without diffusion) to dwarfs from the sample of Fuhrmann (1998) (columns 1–5). Errors according to the original paper are given in the second line for each object. Ages are derived in three steps (groups (1)–(3)): The first one using a mixture with $Y = 0.25$ and the metallicity closest to that of the object (cf. Tab. 1). The second step is to interpolate to the observed metallicity, but still assuming $Y = 0.25$. Finally, full interpolation to the object's metallicity and $Y = 0.235$ is done. For this case, the age uncertainties due to the errors in metallicity, bolometric magnitude and mass ($\triangle t_1$–$\triangle t_3$) are given. All ages (in 10^9 yrs) were obtained from application of Eq. (2), while theoretical effective temperatures, given next to ages, were obtained from the evolutionary tracks. Explanation of remarks: (1) age taken directly from evolutionary tracks: step (1): 8.79; step (3): 10.43 Gyr; (2) $T_{\rm eff}$ taken from 0.6 $M_\odot$-tracks only, since 0.7 $M_\odot$ is always brighter than observed $M_{\rm bol}$; (3) no $T_{\rm eff}$ derived, [Fe/H] being too high.

object	**stellar parameters**				**(1)**		**(2)**		**(3)**					note
	[Fe/H]	$M_{\rm bol}$	$M_\odot$	$T_{\rm eff}$	age	$T_{\rm eff}$	age	$T_{\rm eff}$	age	$T_{\rm eff}$	$\triangle t_1$	$\triangle t_2$	$\triangle t_3$	
HD19445	-1.95	4.91	0.74	6016	10.8	6289	11.3	6243	13.4	6122	±0.2	±1.0	9.9–18.0	
	0.07	0.11	0.037	80									12.5–14.3	
HD45282	-1.52	1.98	0.90	5282	8.9	5321	9.2	5218	10.2	5267	±0.2	±0.1	8.3–12.6	1
	0.06	0.31	0.045	80									9.8–10.6	
HD103095	-1.35	6.33	0.64	5110	8.9	5128	5.8	5195	9.7	5184	±1.5	±1.6	< 18.1	2
	0.10	0.05	0.032	80										
HD194598	-1.12	4.45	0.84	6058	9.3	6232	9.4	6230	11.1	6151	±0.4	±1.0	7.7–15.0	
	0.07	0.16	0.042	80									10.3–11.9	
HD201891	-1.05	4.46	0.81	5943	11.9	—	12.4	—	14.4	—	+1.4	±0.5	10.5–18.7	3
	0.08	0.09	0.041	80										

The derived ages appear to be rather consistent except for the 5.8 Gyr for HD103095 (step 2), which is the most unevolved and least massive object (see Fig. 2 of Fuhrmann 1998). The final ages ($Y = 0.235$) range from 9.7–14.4 and are therefore in rough agreement with cluster ages (Salaris & Weiss 1998) computed with similar models. In the case of HD45282, we can derive the age also directly from the evolutionary tracks for this mass ($0.9\,M_\odot$), i.e. without employing our fit formulae. We then obtain for step 1 8.79 Gyr (compared to 8.9 from Eq. (2); column 6) and 10.43 Gyr compared to 10.2 Gyr (column 10) for the final mixture interpolation. This emphasizes the negligible error due to Eqs. (1) and (2) for these typical ages. In general, we find that ages obtained by linear interpolation between the tracks agree with the fitting formulae results to 5% or better.

Columns 12–14 of Tab. 8 list the age uncertainties resulting from the errors in the observational quantities, which are given in the second lines of columns 2–5. Obviously, the mass uncertainty of 5% (assumed for column 4) is by far too large to allow accurate age determinations. The resulting age range ($\triangle t_3$) is of order 8 Gyr, especially for the lower masses. This emphasizes the need for evolved objects close to or after the turn-off. HD45282 is such an object, beginning already its RGB ascent. For three objects we give $\triangle t_3$ under the assumption that the mass is accurate to 1% (second line of $\triangle t_3$), which would lead to acceptable uncertainties. This is also the achievable accuracy in detached eclipsing binary systems (Paczyński 1997). The age uncertainty due to metallicity ($\triangle t_1$) is almost negligible and that due to brightness – i.e. distance – errors ($\triangle t_2$) of order 1 Gyr or smaller. An exception is HD103095, which, due to its low mass and unevolved state is of course most sensitive. In this case, the upper mass limit of $0.68\,M_\odot$ is actually inconsistent with the lowest (zero-age) brightness of our stellar models. A lower limit for $\triangle t_3$ is therefore missing. HD201891 is outside the metallicity range of our models; its age of 14.4 Gyr, which is the highest of all objects, might be the result of applying Eq. (2) outside its definition range. The upper limit of the metallicity range ($[\mathrm{Fe/H}] = -0.97$) was not explored. For HD194598 the small extrapolation was allowed.

As a further consistency test we derived effective temperatures by interpolating between the tracks. These T_eff are always given in the column following that with the age. The agreement with the observed temperatures is, at least in the final case ($Y = 0.235$) of order of the T_eff-error, with a tendency, however, that our temperatures are higher. This could be an indication that diffusion, which has been ignored here, is indeed active (Salaris et al. 2000). T_eff for HD103095 was derived from the $0.6\,M_\odot$ tracks only for the reasons given in the previous paragraph.

We finally comment on the use of models including diffusion. *Assuming* that the typical metal depletion for a low-mass star of cosmological age is of order 0.3 dex (Salaris et al. 2000), we have applied the $t(L)$-relation of our D-models to HD19445 and HD194598. Then the final (step 3) ages turn out to be 13.6 and 10.7 Gyr, which is slightly older than in the C-case. Effective temperatures are reduced to 5931 resp. 5194 K. Both values are again within the observational uncertainties.

4.3. Conclusions

The comparison with other calculations and the application to (single) stars with determined absolute stellar parameters revealed that the largest errors in age determinations based on our stellar evolution tracks are (1) mass, which must be known to 1% accuracy and (2) systematic uncertainties/differences in and between theretical models.

A physical source of uncertainty concerns the effectiveness of diffusion. In our D–calculations, full diffusion of hydrogen and helium with coefficients calculated following Thoul et al. (1994) was included. This leads in many cases, due to the extremly thin convective envelopes of metal-poor main-sequence stars, to an almost complete depletion of the models in helium, which accumulates below the convective layers. As soon as the star gets cooler, the convective envelope deepens and the helium is mixed back to the surface, as is reflected in the vanishing differences in the HRD in Fig. 3[1]. Salaris et al. (2000) recently have investigated in detail the proper use of isochrones to be fitted to either GC or field halo subdwarf data, when diffusion is included. The main point to be stressed is that the present surface metallicity of an individual subdwarf is not the initial one, but is lower by 0.1–0.4 dex (depending on mass and age) due to diffusion. In a GC, however, [Fe/H] is usually determined from red giants, in which the original surface metallicity has been restored by convection. Here, an evolutionary track with this initial metallicity and diffusion included would be the correct one to be used for an individual star.

---

[1] Very low helium abundances towards the end of the main sequence are found in many comparable calculations, which include diffusion, as we were informed by private communication by S. Degl'Innocenti, S. Cassisi, M. Salaris and I. Mazzitelli.

Arguments in favor of diffusion acting close to how it is calculated are the solar model (Richard et al. 1996; Guenther & Demarque 1997) and the temperatures of main-sequence subgiants with HIPPARCOS-distances, which, according to Morel & Baglin (1999) and Salaris et al. (2000) can be explained by the fact that diffusion leads to lower temperatures (see Fig. 3). Arguments against the full action of sedimentation (rather, arguments in favour of an additional mixing process counteracting diffusion) are the remaining discrepancy between solar models and the seismic Sun just below the convective envelope (Richard et al. 1996) and the presence of ^{7}Li in old metal-poor stars (Vauclair & Charbonnel 1998). In addition, we remark that Morel & Baglin (1999) tried to explain temperature differences of about 100 K, while in metal-poor low-mass stars the effect of diffusion might reduce $T_{\rm eff}$ by 200 K or more. This leads to colours so red that the comparison with the turn-off colour of some globular clusters would yield negative reddening (e.g. M5, for which models without diffusion result in a reddening of only 0.02 mag). We added a few test calculations (for the case $M/M_\odot = 0.8$, $Y = 0.25$, $Z = 0.001$), in which either convective overshooting (as in Schlattl & Weiss 1999) or an enhanced stellar wind (following Vauclair & Charbonnel 1995) or both was employed to reduce the effect of gravitational settling. For pure diffusion a surface helium abundance at the end of the main sequence of $Y_{\rm s} = 10^{-4}$ results; the overshooting models retain up to $Y_{\rm s} = 0.04$, those with a Reimers mass loss ($\eta = 0.4$) $Y_{\rm s} = 0.06$, and those with both effects $Y_{\rm s} = 0.09$. Note that the TO age of this star is only 9.8 Gyr. For a cosmological TO age of about 12 Gyr the mass would be higher and the sedimentation effect smaller due to the larger extend of the convective envelope (see also Salaris et al. 2000).

Without elaborating further on this discussion, the true effectiveness of diffusion might lead to main-sequence lifetimes somewhere between the extremes of no and full diffusion. All arguments brought forward here concern the photospheric properties of stars; however, the evolutionary speed is determined by the central evolution (diffusion leading to a faster aging by adding helium to the core). On the other hand, the processes counteracting diffusion near to the photosphere could do the same at the center (e.g. rotation-induced mixing). Therefore, the true main-sequence life-time might be in between the two limiting cases investigated here; the difference between them being of order 1 Gyr (see Tables A1–A24). A similar result was obtained by Castellani & Degl'Innocenti (1999), who discussed the effect in the case of globular cluster isochrones.

To conclude, we have presented an extensive grid of metal-poor low-mass stellar models. The intention is that these data could be used for determining stellar ages, if global parameters such as mass, luminosity and composition of individual halo or globular cluster stars are known. The data can also be used for standard isochrone construction. To facilitate age derivation, we have presented fitting formulae, which reproduce the evolutionary results with an accuracy of 5% or better for the age range of interest (≈ 10 Gyr). We consider the uncertainty of the evolutionary ages to be of order 1 Gyr (at cosmic ages) due to systematic uncertainties in the models and calculations and another 1 Gyr (at most) due to the unknown effectiveness of diffusion. In this respect, the accuracy of the fitting formulae is within these principal uncertainties.

Application of our fit formulae to five metal-poor (halo) field stars with accurately known metallicity and brightness and reasonably well-determined mass resulted in ages between 9.7 and 13.4 Gyr (except for one star with a metallicity outside our model grid). Such ages appear to be in reasonable agreement with recent globular cluster age determinations (Salaris & Weiss 1998) using similar stellar models. The uncertainties due to metallicity or distance errors are smaller than the model uncertainties, but the 5% mass uncertainty results in an age error of up to ±4 Gyr. A 1% accuracy in mass must be achieved to make this error source comparable to all others. It appears that the use of the fitting formulae does not introduce an additional error source of relevance.

We have not discussed the importance of the effective temperatures, which in the stellar models depend on the convection theory or parameter used. This is because $T_{\rm eff}$ is a very insensitive discriminator between different masses; it should therefore not be used to select the mass of the evolutionary track to be compared. On the other hand, if the stellar mass is known (with some error), most likely the effective temperature of the corresponding track is within the error range. Finally, for known mass, errors in the models' effective temperature do not influence the t–L–relation. This is different from isochrone age determinations, where $T_{\rm eff}$ influences the morphology and therefore the luminosity of the turn-off, as illustrated by Mazzitelli et al. (1995) by using two different convection theories. However, $T_{\rm eff}$-values for stars with determined mass and luminosity will provide independent checks for the quality of the stellar models. Our test application results in effective temperatures, which are within the given uncertainty of the observationally determined ones. This we regard as an encouraging confirmation of our models.

Acknowledgements. The continuing support by B. Paczyński, who stimulated this work, is gratefully acknowledged. We are also indebted to S. Degl'Innocenti and M. Salaris for comparing their results with ours, and to D. Alexander and F. Rogers for providing us with their opacity tables calculated for our particular needs. H. Ritter very diligently read the paper and helped to improve it considerably.

References

Alexander D.R., Ferguson J.W., 1994, ApJ 437, 879
Andersen J., Clausen J.V., Nordström B., Gustafsson B., VandenBerg D.A., 1988, A&A 196, 128
Baraffe I., Chabrier G., Allard F., Hauschildt P.H., 1997, A&A 327, 1054
Bennett P.D., Harper G.H., Brown A., Hummel C.A., 1996, ApJ 471, 454
Cassisi S., Castellani V., Degl'Innocenti S., Weiss A., 1998, A&AS 129, 267
Castellani V., Degl'Innocenti S., Girardi L. et al., 2000, A&A
Castellani V., Degl'Innocenti S., 1999, A&A 344, 97
Caughlan G., Fowler W., 1988, Atomic Data Nuc. Data Tables 40, 283
Chabrier G., Baraffe I., 1995, ApJL 451, L29
D'Antona F., Caloi V., Mazzitelli I., 1997, ApJ 477, 519
Forveille T., Beuzit J.L., Delfosse X. et al., 1999, A&A 351, 619
Fuhrmann K., 1998, A&A 338, 161
Fuhrmann K., 2000, in A. Weiss, T. Abel, and V. Hill (eds.), The First Stars, ESO conference proceedings. Springer, Heidelberg, p. 68
Girardi L., Bressan A., Bertelli G., Chiosi C., 1999, A&AS, submitted
Gratton R.G., Sneden C., Carretta E., Bragaglia A., 2000, A&A 154, 169
Guenther D.B., Demarque P., 1997, ApJ 484, 937
Haft M., Raffelt G., Weiss A., 1994, ApJ 425, 222, Erratum: 438, 1017 [1995]
Iglesias C.A., Rogers F.J., 1996, ApJ 464, 943
Israelian G.I., López R.J.G., Rebolo R., 1998, ApJ 507, 805
Itoh N., Mitake S., Iyetomi H., Ichimaru S., 1983, ApJ 273, 774
Izotov Y.I., Thuan T.X., 1998, ApJ 500, 188
Kaluzny J., Kubiak M., Szymanski M. et al., 1996, A&AS 120, 139
Kaluzny J., Kubiak M., Szymanski M. et al., 1997a, A&AS 122, 471
Kaluzny J., Thompson I.B., Krzeminski W., 1997b, AJ (113), 2219
Kippenhahn R., Weigert A., Hofmeister E., 1967, *Methods for Calculating Stellar Evolution*, vol. 7 of Methods in Computational Physics, 129, New York: Academic Press
Lebreton Y., Perrin M.N., Cayrel R., Baglin A., Fernandes J., 1999, A&A 350, 587
Mazzitelli I., D'Antona F., Caloi V., 1995, A&A 302, 382
Milone E.F., Stagg C.R., Kurucz R.L., 1992, ApJS 79, 123
Morel P., Baglin A., 1999, A&A 345, 156
Munakata H., Kohyama Y., Itoh N., 1985, ApJ 296, 197, Erratum: 304, 580 [1986]
Olive K.A., Steigman G., Skillman E.D., 1997, ApJ 483, 788
Paczyński B., 1997, in M. Livio, M. Donahue, and N. Panagia (eds.), The extragalactic distance scale, vol. 10 of STScI Symposium Series Series. Cambridge University Press, Cambridge

Richard O., Vauclair S., Charbonnel C., Dziembowski W.A., 1996, A&A 312, 1000

Rogers F.J., Swenson F.J., Iglesias C.A., 1996, ApJ 456, 902

Salaris M., Groenewegen M.A.T., Weiss A., 2000, A&A, in press

Salaris M., Straniero O., Chieffi S., 1993, ApJ 414, 580

Salaris M., Weiss A., 1998, A&A 335, 943

Saumon D., Chabrier G., van Horn H.M., 1995, ApJS 99, 713

Schlattl H., 1996, *Numerische und physikalische Genauigkeit von Sonnenmodellen*, Master's thesis, Techn. Univ. München

Schlattl H., 1999, *The Sun, a laboratory for neutrino- and astrophysics*, Ph.D. thesis, Techn. Univ. München

Schlattl H., Weiss A., 1999, A&A 347, 272

Schlattl H., Weiss A., Ludwig H.G., 1997, A&A 322, 646

Schröder K.P., Pols O.R., Eggleton P.P., 1997, MNRAS 285, 696

Spaeth H., 1973, *Spline-Algorithmen zur Konstruktion glatter Kurven und Flächen*, Oldenburg-Verlag, München

Thoul A.A., Bahcall J.N., Loeb A., 1994, ApJ 421, 828

Tout C.A., Pols O.R., Eggleton P.P., Han Z., 1996, MNRAS 281, 257

Vauclair S., Charbonnel C., 1995, A&A 295, 715

Vauclair S., Charbonnel C., 1998, ApJ 502, 372

Wagenhuber J., 1996, *Entwicklung von Sternen verschiedener Massen und Metallizitäten auf dem asymptotischen Riesenast und danach*, Ph.D. thesis, Techn. Univ. München

Wagenhuber J., Weiss A., 1994, A&A 286, 121

Weiss A., 1987, A&A 185, 165

Weiss A., Salaris M., 1999, A&A 346, 897

Appendix A: Tables containing evolutionary data

The evolutionary properties for *all* evolutionary models calculated. They are given as Tables A1–A24 (A1–A12 for the (canonical) case "C" without diffusion and A13–A24 for case "D", the one including diffusion in the same form as Tab. A1 (which is the table for the C-case composition $(Y, Z) = (0.20, 0.0001)$). The columns relate to:

1. age (in 10^9 years)
2. $\log L/L_\odot$;
3. $\log T_{\rm eff}$;
4. central helium abundance $Y_{\rm c}$ or relative mass of the hydrogen-exhausted core, $m_{\rm hc}$; the switching between the two quantities is easily recognizable by the jump from a number close to 1 to one of order 0.2;
5. surface helium abundance $Y_{\rm s}$;
6. $m_{\rm ce}$, the location of the bottom of the convective envelope in relative mass coordinate; $m_{\rm ce} = 1.0$ corresponds to a convective envelope of thickness $< 10^{-4} M_r/M$ or to a completely radiative envelope. In a few cases, the very last model exhibits already a convective shell in the helium flash region. In these cases, this column gives the bottom of this inner convective region and the value listed is of order 0.2 or smaller;
7. relative mass of the convective core, $m_{\rm cc}$.

The tables are an extract of the full evolutionary results, such that sufficiently, but not too many time-steps are provided. They contain the most important stages, like ZAMS, turn-off and tip of the RGB. The complete set of data can be obtained from the authors on request.

Table A1. Evolution of models without diffusion (C-case) of composition $(Y, Z) = (0.20, 0.001)$

Age	$\log L/L_\odot$	$\lg T_{\rm eff}$	$Y_{\rm c}/m_{\rm hc}$	$Y_{\rm s}$	$m_{\rm ce}$	$m_{\rm cc}$
$M = 0.6\ M_\odot$						
0.000E+00	-0.8711	3.7071	0.2000	0.200	0.8967	0.0026
3.308E+08	-0.8662	3.7045	0.2052	0.200	0.8792	0.0690
1.075E+10	-0.7727	3.7147	0.4375	0.200	0.9081	0.0000
1.975E+10	-0.6792	3.7250	0.6434	0.200	0.9323	0.0000
2.694E+10	-0.5794	3.7351	0.7968	0.200	0.9526	0.0000
3.231E+10	-0.4789	3.7454	0.8988	0.200	0.9627	0.0000
3.634E+10	-0.3772	3.7541	0.9521	0.200	0.9716	0.0000
3.927E+10	-0.2747	3.7608	0.9751	0.200	0.9755	0.0000
4.137E+10	-0.1724	3.7652	0.9868	0.200	0.9790	0.0000
4.298E+10	-0.0697	3.7668	0.2154	0.200	0.9818	0.0000
4.409E+10	0.0315	3.7658	0.2361	0.200	0.9790	0.0000
4.481E+10	0.1329	3.7601	0.2517	0.200	0.9661	0.0000
4.524E+10	0.2338	3.7507	0.2622	0.200	0.9322	0.0000
4.553E+10	0.3345	3.7417	0.2702	0.200	0.8640	0.0000
4.575E+10	0.4371	3.7357	0.2792	0.200	0.7885	0.0000
4.594E+10	0.5377	3.7322	0.2914	0.200	0.7269	0.0000
4.612E+10	0.6377	3.7296	0.3075	0.200	0.6821	0.0000
4.626E+10	0.7388	3.7273	0.3255	0.201	0.6482	0.0000
4.638E+10	0.8398	3.7250	0.3432	0.201	0.6204	0.0000
4.647E+10	0.9406	3.7227	0.3617	0.201	0.5982	0.0000
4.655E+10	1.0410	3.7203	0.3794	0.202	0.5819	0.0000
4.661E+10	1.1414	3.7178	0.3971	0.202	0.5712	0.0000
4.666E+10	1.2415	3.7150	0.4143	0.202	0.5658	0.0000
4.670E+10	1.3419	3.7122	0.4312	0.202	0.5631	0.0000
4.673E+10	1.4420	3.7093	0.4479	0.202	0.5631	0.0000
4.676E+10	1.5422	3.7062	0.4648	0.202	0.5657	0.0000
4.678E+10	1.6423	3.7031	0.4821	0.202	0.5710	0.0000
4.679E+10	1.7425	3.6998	0.4997	0.202	0.5790	0.0000
4.681E+10	1.8426	3.6961	0.5174	0.202	0.5883	0.0000
4.682E+10	1.9427	3.6927	0.5359	0.202	0.5992	0.0000
4.683E+10	2.0427	3.6893	0.5570	0.202	0.6144	0.0000
4.684E+10	2.1428	3.6857	0.5755	0.202	0.6282	0.0000
4.684E+10	2.2430	3.6821	0.5948	0.202	0.6421	0.0000
4.685E+10	2.3431	3.6784	0.6148	0.202	0.6576	0.0000
4.685E+10	2.4432	3.6746	0.6356	0.202	0.6745	0.0000
4.686E+10	2.5434	3.6707	0.6574	0.202	0.6927	0.0000
4.686E+10	2.6435	3.6667	0.6803	0.202	0.7123	0.0000
4.686E+10	2.7437	3.6626	0.7039	0.202	0.7334	0.0000
4.686E+10	2.8438	3.6583	0.7280	0.202	0.7547	0.0000
4.687E+10	2.9440	3.6539	0.7494	0.202	0.7733	0.0000
4.687E+10	3.0441	3.6495	0.7736	0.202	0.7950	0.0000
4.687E+10	3.1443	3.6452	0.7984	0.202	0.8175	0.0000
4.687E+10	3.2445	3.6411	0.8240	0.202	0.8411	0.0000
4.687E+10	3.3210	3.6383	0.8435	0.202	0.8592	0.0000
$M = 0.7\ M_\odot$						
0.000E+00	-0.5366	3.7473	0.2003	0.200	0.9748	0.1191
1.772E+08	-0.5766	3.7382	0.2046	0.200	0.9621	0.0642
5.700E+09	-0.4884	3.7485	0.3920	0.200	0.9732	0.0000
1.078E+10	-0.3992	3.7589	0.5948	0.200	0.9802	0.0000
1.528E+10	-0.2991	3.7688	0.7709	0.200	0.9866	0.0000
1.875E+10	-0.1978	3.7763	0.8909	0.200	0.9916	0.0000
2.127E+10	-0.0951	3.7829	0.9469	0.200	0.9943	0.0000
2.305E+10	0.0075	3.7874	0.9719	0.200	0.9959	0.0000
2.435E+10	0.1081	3.7899	0.9905	0.200	0.9969	0.0000
2.535E+10	0.2106	3.7893	0.2108	0.200	0.9971	0.0000
2.601E+10	0.3127	3.7825	0.2301	0.200	0.9953	0.0000
2.632E+10	0.3858	3.7720	0.2400	0.200	0.9877	0.0000
2.648E+10	0.4387	3.7614	0.2451	0.200	0.9690	0.0000
2.661E+10	0.4915	3.7511	0.2489	0.200	0.9273	0.0000
2.674E+10	0.5734	3.7410	0.2533	0.200	0.8408	0.0000
2.687E+10	0.6751	3.7346	0.2599	0.200	0.7469	0.0000
2.698E+10	0.7766	3.7307	0.2709	0.201	0.6742	0.0000
2.707E+10	0.8767	3.7277	0.2855	0.201	0.6166	0.0000
2.715E+10	0.9776	3.7249	0.3015	0.202	0.5782	0.0000
2.722E+10	1.0782	3.7222	0.3179	0.202	0.5467	0.0000
2.728E+10	1.1789	3.7195	0.3341	0.203	0.5281	0.0000
2.732E+10	1.2792	3.7167	0.3500	0.203	0.5098	0.0000
2.736E+10	1.3796	3.7138	0.3654	0.203	0.5006	0.0000
2.738E+10	1.4800	3.7107	0.3807	0.203	0.4976	0.0000
2.741E+10	1.5801	3.7076	0.3960	0.203	0.4975	0.0000
2.743E+10	1.6803	3.7044	0.4115	0.203	0.5005	0.0000
2.744E+10	1.7804	3.7011	0.4273	0.203	0.5035	0.0000
2.745E+10	1.8807	3.6973	0.4435	0.203	0.5095	0.0000
2.747E+10	1.9809	3.6938	0.4601	0.203	0.5186	0.0000
2.747E+10	2.0811	3.6903	0.4777	0.203	0.5293	0.0000
2.748E+10	2.1813	3.6868	0.4992	0.203	0.5463	0.0000
2.749E+10	2.2814	3.6831	0.5156	0.203	0.5580	0.0000
2.749E+10	2.3814	3.6793	0.5328	0.203	0.5713	0.0000
2.750E+10	2.4815	3.6754	0.5509	0.203	0.5856	0.0000
2.750E+10	2.5816	3.6714	0.5699	0.203	0.6016	0.0000
2.750E+10	2.6816	3.6673	0.5897	0.203	0.6177	0.0000
2.751E+10	2.7817	3.6631	0.6100	0.203	0.6356	0.0000
2.751E+10	2.8817	3.6586	0.6290	0.203	0.6518	0.0000
2.751E+10	2.9818	3.6539	0.6490	0.203	0.6693	0.0000
2.751E+10	3.0820	3.6492	0.6697	0.203	0.6878	0.0000
2.751E+10	3.1821	3.6444	0.6914	0.203	0.7075	0.0000
2.751E+10	3.2823	3.6395	0.7131	0.203	0.7275	0.0000
2.751E+10	3.3165	3.6379	0.7206	0.203	0.7343	0.0000

Table A1. (contd.)

Age	$\log L/L_\odot$	$\lg T_{\rm eff}$	$Y_{\rm c}/m_{\rm hc}$	$Y_{\rm s}$	$m_{\rm ce}$	$m_{\rm cc}$
$M = 0.8\,M_\odot$						
0.000E+00	-0.2959	3.7834	0.2000	0.200	0.9950	0.0828
1.031E+08	-0.3076	3.7737	0.2042	0.200	0.9908	0.0559
4.127E+09	-0.2068	3.7838	0.4347	0.200	0.9950	0.0000
7.556E+09	-0.1064	3.7933	0.6599	0.200	0.9973	0.0000
1.018E+10	-0.0056	3.8011	0.8284	0.200	0.9986	0.0000
1.206E+10	0.0946	3.8074	0.9159	0.200	0.9993	0.0000
1.340E+10	0.1947	3.8122	0.9554	0.200	0.9996	0.0000
1.441E+10	0.2950	3.8151	0.9843	0.200	0.9997	0.0000
1.517E+10	0.3955	3.8146	0.1932	0.200	0.9997	0.0000
1.568E+10	0.4963	3.8061	0.2144	0.200	0.9996	0.0000
1.587E+10	0.5485	3.7960	0.2227	0.200	0.9993	0.0000
1.597E+10	0.5843	3.7858	0.2272	0.200	0.9980	0.0000
1.604E+10	0.6136	3.7756	0.2301	0.200	0.9937	0.0000
1.610E+10	0.6408	3.7652	0.2323	0.200	0.9819	0.0000
1.615E+10	0.6707	3.7550	0.2341	0.200	0.9495	0.0000
1.621E+10	0.7177	3.7450	0.2360	0.200	0.8792	0.0000
1.630E+10	0.8185	3.7357	0.2397	0.200	0.7525	0.0000
1.637E+10	0.9191	3.7308	0.2466	0.201	0.6552	0.0000
1.643E+10	1.0195	3.7273	0.2586	0.201	0.5846	0.0000
1.649E+10	1.1200	3.7242	0.2729	0.202	0.5344	0.0000
1.653E+10	1.2203	3.7212	0.2875	0.203	0.4978	0.0000
1.657E+10	1.3209	3.7182	0.3019	0.204	0.4736	0.0000
1.660E+10	1.4209	3.7152	0.3161	0.204	0.4560	0.0000
1.663E+10	1.5212	3.7121	0.3302	0.205	0.4472	0.0000
1.665E+10	1.6213	3.7089	0.3443	0.205	0.4443	0.0000
1.667E+10	1.7215	3.7057	0.3585	0.205	0.4442	0.0000
1.668E+10	1.8216	3.7023	0.3730	0.205	0.4471	0.0000
1.669E+10	1.9217	3.6984	0.3878	0.205	0.4500	0.0000
1.670E+10	2.0220	3.6949	0.4030	0.205	0.4572	0.0000
1.671E+10	2.1222	3.6913	0.4188	0.205	0.4658	0.0000
1.672E+10	2.2223	3.6879	0.4426	0.205	0.4868	0.0000
1.673E+10	2.3224	3.6841	0.4569	0.205	0.4951	0.0000
1.673E+10	2.4226	3.6802	0.4722	0.205	0.5064	0.0000
1.673E+10	2.5227	3.6763	0.4883	0.205	0.5193	0.0000
1.674E+10	2.6228	3.6723	0.5052	0.205	0.5323	0.0000
1.674E+10	2.7229	3.6681	0.5226	0.205	0.5474	0.0000
1.674E+10	2.8229	3.6638	0.5403	0.205	0.5626	0.0000
1.674E+10	2.9230	3.6592	0.5569	0.205	0.5768	0.0000
1.674E+10	3.0231	3.6545	0.5747	0.205	0.5923	0.0000
1.675E+10	3.1231	3.6496	0.5932	0.205	0.6088	0.0000
1.675E+10	3.2233	3.6446	0.6121	0.205	0.6258	0.0000
1.675E+10	3.3113	3.6402	0.6287	0.205	0.6409	0.0000
$M = 0.9\,M_\odot$						
0.000E+00	-0.0712	3.8094	0.2000	0.200	0.9992	0.1091
1.088E+08	-0.0713	3.8036	0.2065	0.200	0.9988	0.0543
2.919E+09	0.0295	3.8138	0.4335	0.200	0.9995	0.0000
5.271E+09	0.1304	3.8227	0.6745	0.200	0.9997	0.0000
7.046E+09	0.2323	3.8304	0.8425	0.200	0.9998	0.0000
8.314E+09	0.3352	3.8372	0.9209	0.200	0.9998	0.0000
9.224E+09	0.4366	3.8425	0.9646	0.200	1.0000	0.0000
9.929E+09	0.5372	3.8448	0.1724	0.200	1.0000	0.0000
1.042E+10	0.6380	3.8379	0.1979	0.200	1.0000	0.0000
1.060E+10	0.6895	3.8272	0.2080	0.200	0.9998	0.0000
1.069E+10	0.7230	3.8168	0.2132	0.200	0.9998	0.0000
1.075E+10	0.7494	3.8063	0.2165	0.200	0.9998	0.0000
1.080E+10	0.7726	3.7953	0.2188	0.200	0.9995	0.0000
1.083E+10	0.7916	3.7850	0.2204	0.200	0.9986	0.0000
1.086E+10	0.8092	3.7743	0.2217	0.200	0.9950	0.0000
1.089E+10	0.8250	3.7639	0.2227	0.200	0.9835	0.0000
1.092E+10	0.8443	3.7536	0.2236	0.200	0.9495	0.0000
1.095E+10	0.8840	3.7434	0.2246	0.200	0.8666	0.0000
1.101E+10	0.9842	3.7340	0.2266	0.200	0.7150	0.0000
1.106E+10	1.0845	3.7292	0.2314	0.201	0.6103	0.0000
1.110E+10	1.1855	3.7255	0.2422	0.202	0.5345	0.0000
1.114E+10	1.2863	3.7222	0.2550	0.204	0.4797	0.0000
1.117E+10	1.3867	3.7190	0.2680	0.205	0.4444	0.0000
1.119E+10	1.4873	3.7158	0.2811	0.206	0.4217	0.0000
1.121E+10	1.5878	3.7126	0.2941	0.206	0.4106	0.0000
1.123E+10	1.6878	3.7094	0.3071	0.207	0.4023	0.0000
1.125E+10	1.7881	3.7060	0.3203	0.207	0.3995	0.0000
1.126E+10	1.8881	3.7025	0.3339	0.207	0.4022	0.0000
1.127E+10	1.9884	3.6986	0.3477	0.207	0.4050	0.0000
1.128E+10	2.0885	3.6950	0.3619	0.207	0.4104	0.0000
1.128E+10	2.1887	3.6914	0.3766	0.207	0.4187	0.0000
1.129E+10	2.2889	3.6879	0.4020	0.207	0.4413	0.0000
1.130E+10	2.3889	3.6840	0.4151	0.207	0.4491	0.0000
1.130E+10	2.4891	3.6801	0.4291	0.207	0.4592	0.0000
1.130E+10	2.5892	3.6761	0.4437	0.207	0.4702	0.0000
1.131E+10	2.6893	3.6720	0.4589	0.207	0.4830	0.0000
1.131E+10	2.7894	3.6678	0.4744	0.207	0.4958	0.0000
1.131E+10	2.8895	3.6633	0.4896	0.207	0.5086	0.0000
1.131E+10	2.9895	3.6587	0.5050	0.207	0.5219	0.0000
1.131E+10	3.0898	3.6539	0.5214	0.207	0.5361	0.0000
1.131E+10	3.1901	3.6489	0.5380	0.207	0.5509	0.0000
1.132E+10	3.2903	3.6438	0.5548	0.207	0.5661	0.0000
1.132E+10	3.3799	3.6391	0.5705	0.207	0.1554	0.0000

Table A1. (contd.)

Age	$\log L/L_\odot$	$\lg T_{\rm eff}$	$Y_{\rm c}/m_{\rm hc}$	$Y_{\rm s}$	$m_{\rm ce}$	$m_{\rm cc}$
$M = 1.0\,M_\odot$						
0.000E+00	0.1257	3.8330	0.2000	0.200	0.9998	0.1296
1.088E+08	0.1379	3.8327	0.2092	0.200	0.9998	0.0575
1.907E+09	0.2274	3.8429	0.4011	0.200	0.9998	0.0014
3.647E+09	0.3305	3.8531	0.6710	0.200	1.0000	0.0000
4.906E+09	0.4331	3.8633	0.8411	0.200	1.0000	0.0000
5.748E+09	0.5290	3.8735	0.9178	0.200	1.0000	0.0000
6.449E+09	0.6315	3.8819	0.9810	0.200	1.0000	0.0000
6.977E+09	0.7343	3.8824	0.1740	0.200	1.0000	0.0000
7.246E+09	0.8113	3.8720	0.1925	0.200	1.0000	0.0000
7.337E+09	0.8463	3.8613	0.1989	0.200	1.0000	0.0000
7.391E+09	0.8712	3.8500	0.2027	0.200	1.0000	0.0000
7.423E+09	0.8885	3.8398	0.2050	0.200	1.0000	0.0000
7.449E+09	0.9043	3.8289	0.2067	0.200	1.0000	0.0000
7.472E+09	0.9195	3.8176	0.2082	0.200	0.9998	0.0000
7.491E+09	0.9327	3.8075	0.2093	0.200	0.9998	0.0000
7.509E+09	0.9461	3.7967	0.2103	0.200	0.9997	0.0000
7.525E+09	0.9579	3.7862	0.2110	0.200	0.9993	0.0000
7.539E+09	0.9684	3.7756	0.2117	0.200	0.9973	0.0000
7.555E+09	0.9777	3.7649	0.2123	0.200	0.9892	0.0000
7.571E+09	0.9881	3.7542	0.2128	0.200	0.9597	0.0000
7.593E+09	1.0142	3.7439	0.2133	0.200	0.8822	0.0000
7.631E+09	1.1026	3.7338	0.2144	0.200	0.7150	0.0000
7.665E+09	1.2035	3.7285	0.2170	0.201	0.5910	0.0000
7.696E+09	1.3045	3.7247	0.2257	0.203	0.5040	0.0000
7.722E+09	1.4049	3.7212	0.2370	0.205	0.4503	0.0000
7.745E+09	1.5053	3.7179	0.2488	0.206	0.4107	0.0000
7.764E+09	1.6059	3.7146	0.2607	0.208	0.3867	0.0000
7.779E+09	1.7063	3.7113	0.2726	0.208	0.3746	0.0000
7.793E+09	1.8067	3.7078	0.2849	0.209	0.3665	0.0000
7.804E+09	1.9067	3.7043	0.2974	0.209	0.3665	0.0000
7.813E+09	2.0069	3.7007	0.3101	0.209	0.3678	0.0000
7.821E+09	2.1070	3.6968	0.3232	0.209	0.3718	0.0000
7.827E+09	2.2073	3.6931	0.3365	0.209	0.3771	0.0000
7.833E+09	2.3074	3.6893	0.3514	0.209	0.3855	0.0000
7.842E+09	2.4076	3.6857	0.3762	0.209	0.4083	0.0000
7.846E+09	2.5077	3.6818	0.3887	0.209	0.4166	0.0000
7.849E+09	2.6078	3.6777	0.4018	0.209	0.4263	0.0000
7.851E+09	2.7079	3.6736	0.4154	0.209	0.4377	0.0000
7.853E+09	2.8080	3.6694	0.4293	0.209	0.4487	0.0000
7.855E+09	2.9081	3.6650	0.4429	0.209	0.4599	0.0000
7.856E+09	3.0082	3.6603	0.4569	0.209	0.4720	0.0000
7.858E+09	3.1083	3.6556	0.4718	0.209	0.4850	0.0000
7.859E+09	3.2084	3.6506	0.4868	0.209	0.4982	0.0000
7.859E+09	3.2948	3.6462	0.4996	0.209	0.5097	0.0000
$M = 1.1\,M_\odot$						
0.000E+00	0.3019	3.8562	0.2000	0.200	1.0000	0.1466
1.317E+08	0.3258	3.8631	0.2145	0.200	1.0000	0.0673
1.185E+09	0.3939	3.8737	0.3469	0.200	1.0000	0.0294
2.105E+09	0.4622	3.8838	0.5187	0.200	1.0000	0.0020
2.973E+09	0.5409	3.8940	0.7225	0.200	1.0000	0.0000
3.643E+09	0.6205	3.9041	0.8441	0.200	1.0000	0.0000
4.281E+09	0.7177	3.9144	0.9355	0.200	1.0000	0.0000
4.810E+09	0.8183	3.9192	0.1482	0.200	1.0000	0.0000
5.164E+09	0.9207	3.9136	0.1771	0.200	1.0000	0.0000
5.280E+09	0.9698	3.9027	0.1873	0.200	1.0000	0.0000
5.336E+09	0.9995	3.8912	0.1921	0.200	1.0000	0.0000
5.368E+09	1.0206	3.8795	0.1949	0.200	1.0000	0.0000
5.389E+09	1.0355	3.8687	0.1966	0.200	1.0000	0.0000
5.405E+09	1.0487	3.8570	0.1979	0.200	1.0000	0.0000
5.416E+09	1.0587	3.8461	0.1987	0.200	1.0000	0.0000
5.426E+09	1.0679	3.8348	0.1994	0.200	1.0000	0.0000
5.434E+09	1.0753	3.8247	0.2000	0.200	1.0000	0.0000
5.442E+09	1.0833	3.8136	0.2005	0.200	0.9998	0.0000
5.451E+09	1.0920	3.8020	0.2010	0.200	0.9998	0.0000
5.459E+09	1.1000	3.7908	0.2015	0.200	0.9997	0.0000
5.468E+09	1.1069	3.7799	0.2019	0.200	0.9990	0.0000
5.477E+09	1.1118	3.7695	0.2023	0.200	0.9956	0.0000
5.486E+09	1.1151	3.7591	0.2026	0.200	0.9827	0.0000
5.498E+09	1.1217	3.7489	0.2029	0.200	0.9386	0.0000
5.515E+09	1.1560	3.7388	0.2033	0.200	0.8233	0.0000
5.545E+09	1.2567	3.7305	0.2042	0.201	0.6429	0.0000
5.569E+09	1.3575	3.7259	0.2078	0.202	0.5284	0.0000
5.590E+09	1.4583	3.7222	0.2169	0.204	0.4504	0.0000
5.609E+09	1.5587	3.7187	0.2273	0.207	0.3997	0.0000
5.625E+09	1.6593	3.7153	0.2382	0.208	0.3720	0.0000
5.638E+09	1.7597	3.7118	0.2493	0.210	0.3508	0.0000
5.650E+09	1.8598	3.7084	0.2607	0.210	0.3403	0.0000
5.659E+09	1.9598	3.7048	0.2724	0.211	0.3377	0.0000
5.667E+09	2.0600	3.7011	0.2842	0.211	0.3377	0.0000
5.674E+09	2.1602	3.6971	0.2963	0.211	0.3415	0.0000
5.680E+09	2.2604	3.6934	0.3086	0.211	0.3467	0.0000
5.685E+09	2.3605	3.6895	0.3225	0.211	0.3532	0.0000
5.694E+09	2.4607	3.6859	0.3484	0.211	0.3770	0.0000
5.697E+09	2.5608	3.6820	0.3599	0.211	0.3849	0.0000
5.700E+09	2.6609	3.6779	0.3718	0.211	0.3938	0.0000
5.702E+09	2.7611	3.6737	0.3842	0.211	0.4035	0.0000
5.704E+09	2.8612	3.6694	0.3972	0.211	0.4145	0.0000
5.705E+09	2.9614	3.6650	0.4093	0.211	0.4245	0.0000
5.707E+09	3.0618	3.6603	0.4225	0.211	0.4359	0.0000
5.708E+09	3.1620	3.6554	0.4362	0.211	0.4476	0.0000
5.709E+09	3.2623	3.6504	0.4496	0.211	0.4595	0.0000
5.709E+09	3.2886	3.6491	0.4532	0.211	0.4628	0.0000

Table A1. (contd.)

Age	$\log L/L_\odot$	$\lg T_{\rm eff}$	$Y_{\rm c}/m_{\rm hc}$	$Y_{\rm s}$	$m_{\rm ce}$	$m_{\rm cc}$
$M = 1.2\,M_\odot$						
0.000E+00	0.4853	3.8990	0.2000	0.200	1.0000	0.1497
1.089E+09	0.5639	3.9094	0.3474	0.200	1.0000	0.0655
1.773E+09	0.6281	3.9195	0.4827	0.200	1.0000	0.0394
2.358E+09	0.6987	3.9298	0.6531	0.200	1.0000	0.0000
2.895E+09	0.7807	3.9400	0.8283	0.200	1.0000	0.0000
3.427E+09	0.8812	3.9485	0.9741	0.200	1.0000	0.0000
3.636E+09	0.9312	3.9505	0.1344	0.200	1.0000	0.0000
3.944E+09	1.0335	3.9467	0.1649	0.200	1.0000	0.0000
4.058E+09	1.0895	3.9361	0.1770	0.200	1.0000	0.0000
4.104E+09	1.1185	3.9258	0.1819	0.200	1.0000	0.0000
4.132E+09	1.1396	3.9149	0.1848	0.200	1.0000	0.0000
4.152E+09	1.1567	3.9032	0.1868	0.200	1.0000	0.0000
4.165E+09	1.1697	3.8918	0.1881	0.200	1.0000	0.0000
4.175E+09	1.1803	3.8805	0.1890	0.200	1.0000	0.0000
4.183E+09	1.1891	3.8693	0.1897	0.200	1.0000	0.0000
4.189E+09	1.1968	3.8579	0.1902	0.200	1.0000	0.0000
4.195E+09	1.2035	3.8461	0.1906	0.200	1.0000	0.0000
4.199E+09	1.2086	3.8359	0.1909	0.200	1.0000	0.0000
4.203E+09	1.2135	3.8252	0.1912	0.200	1.0000	0.0000
4.206E+09	1.2179	3.8149	0.1915	0.200	1.0000	0.0000
4.211E+09	1.2226	3.8038	0.1917	0.200	0.9998	0.0000
4.216E+09	1.2274	3.7923	0.1920	0.200	0.9997	0.0000
4.221E+09	1.2310	3.7817	0.1923	0.200	0.9994	0.0000
4.226E+09	1.2328	3.7714	0.1925	0.200	0.9977	0.0000
4.232E+09	1.2318	3.7608	0.1928	0.200	0.9896	0.0000
4.240E+09	1.2300	3.7507	0.1930	0.200	0.9597	0.0000
4.251E+09	1.2446	3.7405	0.1933	0.200	0.8600	0.0000
4.275E+09	1.3426	3.7304	0.1939	0.201	0.6429	0.0000
4.294E+09	1.4435	3.7256	0.1966	0.202	0.5161	0.0000
4.310E+09	1.5439	3.7217	0.2044	0.205	0.4332	0.0000
4.325E+09	1.6441	3.7181	0.2138	0.207	0.3774	0.0000
4.338E+09	1.7442	3.7147	0.2238	0.210	0.3456	0.0000
4.349E+09	1.8446	3.7111	0.2343	0.211	0.3277	0.0000
4.359E+09	1.9448	3.7075	0.2450	0.212	0.3176	0.0000
4.367E+09	2.0449	3.7039	0.2560	0.212	0.3151	0.0000
4.373E+09	2.1451	3.7001	0.2670	0.212	0.3151	0.0000
4.379E+09	2.2452	3.6961	0.2782	0.212	0.3175	0.0000
4.383E+09	2.3454	3.6923	0.2900	0.212	0.3224	0.0000
4.393E+09	2.4456	3.6887	0.3186	0.212	0.3479	0.0000
4.396E+09	2.5457	3.6847	0.3287	0.212	0.3538	0.0000
4.399E+09	2.6459	3.6806	0.3394	0.212	0.3610	0.0000
4.401E+09	2.7460	3.6765	0.3507	0.212	0.3696	0.0000
4.403E+09	2.8461	3.6722	0.3624	0.212	0.3790	0.0000
4.405E+09	2.9462	3.6678	0.3737	0.212	0.3882	0.0000
4.406E+09	3.0462	3.6633	0.3857	0.212	0.3985	0.0000
4.407E+09	3.1464	3.6585	0.3979	0.212	0.4089	0.0000
4.408E+09	3.2473	3.6535	0.4103	0.212	0.4197	0.0000
4.409E+09	3.3395	3.6489	0.4225	0.212	0.0978	0.0000
$M = 1.3\,M_\odot$						
0.000E+00	0.6437	3.9350	0.2006	0.200	1.0000	0.0856
1.017E+08	0.6374	3.9278	0.2147	0.200	1.0000	0.1170
8.388E+08	0.7009	3.9384	0.3248	0.200	1.0000	0.0938
1.474E+09	0.7684	3.9490	0.4575	0.200	1.0000	0.0689
1.953E+09	0.8353	3.9594	0.5987	0.200	1.0000	0.0324
2.339E+09	0.9086	3.9695	0.7877	0.200	1.0000	0.0000
2.782E+09	1.0098	3.9769	0.9912	0.200	1.0000	0.0000
3.076E+09	1.1108	3.9778	0.1453	0.200	1.0000	0.0000
3.234E+09	1.1924	3.9673	0.1654	0.200	1.0000	0.0000
3.280E+09	1.2257	3.9569	0.1714	0.200	1.0000	0.0000
3.306E+09	1.2479	3.9463	0.1748	0.200	1.0000	0.0000
3.323E+09	1.2652	3.9351	0.1769	0.200	1.0000	0.0000
3.334E+09	1.2784	3.9240	0.1782	0.200	1.0000	0.0000
3.342E+09	1.2883	3.9139	0.1792	0.200	1.0000	0.0000
3.349E+09	1.2973	3.9028	0.1799	0.200	1.0000	0.0000
3.355E+09	1.3055	3.8909	0.1805	0.200	1.0000	0.0000
3.360E+09	1.3124	3.8789	0.1810	0.200	1.0000	0.0000
3.363E+09	1.3179	3.8677	0.1813	0.200	1.0000	0.0000
3.367E+09	1.3227	3.8562	0.1816	0.200	1.0000	0.0000
3.370E+09	1.3267	3.8451	0.1818	0.200	1.0000	0.0000
3.372E+09	1.3301	3.8334	0.1820	0.200	1.0000	0.0000
3.375E+09	1.3329	3.8228	0.1822	0.200	1.0000	0.0000
3.377E+09	1.3355	3.8113	0.1824	0.200	1.0000	0.0000
3.380E+09	1.3376	3.8006	0.1825	0.200	0.9998	0.0000
3.383E+09	1.3394	3.7895	0.1827	0.200	0.9998	0.0000
3.386E+09	1.3397	3.7787	0.1829	0.200	0.9994	0.0000
3.390E+09	1.3374	3.7682	0.1831	0.200	0.9975	0.0000
3.395E+09	1.3315	3.7578	0.1832	0.200	0.9877	0.0000
3.400E+09	1.3252	3.7477	0.1834	0.200	0.9495	0.0000
3.410E+09	1.3446	3.7376	0.1837	0.200	0.8281	0.0000
3.429E+09	1.4458	3.7288	0.1845	0.201	0.6103	0.0000
3.444E+09	1.5468	3.7242	0.1885	0.203	0.4859	0.0000
3.457E+09	1.6471	3.7203	0.1962	0.206	0.4053	0.0000
3.469E+09	1.7476	3.7167	0.2051	0.209	0.3509	0.0000
3.479E+09	1.8478	3.7131	0.2146	0.211	0.3201	0.0000
3.488E+09	1.9478	3.7095	0.2245	0.212	0.3029	0.0000
3.496E+09	2.0481	3.7058	0.2346	0.213	0.2957	0.0000
3.502E+09	2.1482	3.7021	0.2447	0.213	0.2945	0.0000
3.508E+09	2.2485	3.6980	0.2552	0.213	0.2957	0.0000
3.512E+09	2.3487	3.6942	0.2660	0.213	0.2992	0.0000
3.516E+09	2.4489	3.6902	0.2776	0.213	0.3040	0.0000
3.525E+09	2.5490	3.6866	0.3043	0.213	0.3287	0.0000
3.527E+09	2.6492	3.6825	0.3140	0.213	0.3350	0.0000
3.529E+09	2.7492	3.6783	0.3243	0.213	0.3426	0.0000
3.531E+09	2.8494	3.6741	0.3352	0.213	0.3511	0.0000
3.533E+09	2.9495	3.6698	0.3457	0.213	0.3593	0.0000
3.534E+09	3.0498	3.6652	0.3567	0.213	0.3686	0.0000
3.535E+09	3.1498	3.6605	0.3680	0.213	0.3783	0.0000
3.536E+09	3.2499	3.6556	0.3793	0.213	0.3881	0.0000
3.537E+09	3.3210	3.6521	0.3881	0.213	0.0781	0.0000